

## Asymptotic sets in networks of coupled quadratic nodes

ANCA RĂDULESCU<sup>†</sup> AND SIMONE EVANS

*Department of Mathematics, State University of New York at New Paltz, New Paltz, NY 12561, USA*

<sup>†</sup>Corresponding author. Email: radulesa@newpaltz.edu

Edited by: Mattia Frasca

[Received on 28 March 2018; editorial decision on 27 July 2018; accepted on 3 August 2018]

We study asymptotic behaviour in networks of  $n$  nodes with discrete quadratic dynamics. While single map complex quadratic iterations have been studied over the past century, considering ensembles of such functions, organized as coupled nodes in an oriented network, generates new questions with potentially interesting applications to the life sciences. We discuss extensions of traditional results from single map iterations, such as the existence of an escape radius; we then investigate whether crucial information about the network is encoded in the behaviour of the critical orbit. We use two previously defined objects: the network Mandelbrot set (i.e., the set of quadratic parameters in  $\mathbb{C}^n$  for which the network is post-critically bounded in  $\mathbb{C}^n$ ) and the equi-M set (the diagonal slice of the network Mandelbrot set, corresponding to all nodes using the identical quadratic map). Using a combination of analytical techniques and numerical simulations, we study topological properties of the equi-M set, with the aim of understanding which of these properties are affected by altering different aspects of the network architecture and node-to-node connectivity strengths. We find that, while equi-M sets no longer have a hyperbolic bulb structure, some of their geometric landmarks (e.g., the cusp) are preserved for any network configuration, and other properties (such as connectedness) depend on the network structure. We further study the relationship between the Mandelbrot set and the connectedness locus of the network uni-Julia set (defined as the set of  $z_0 \in \mathbb{C}$  for which all nodes remain bounded when they are all initialed identically at  $z_0$ ). We discuss using the geometry of uni-Julia or equi-M sets to classify asymptotic behaviour in networks based on their underlying graph structure. Finally, we propose using a form of averaging uni-Julia and equi-M sets to describe statistically the likelihood of a specific asymptotic behaviour, considered over an entire collection of configurations. We discuss which analytical results can be further supported or refined in the future. We also revisit the ties with applications to the life sciences. We explore how this theoretical study may inform on using similar methods to understand natural systems with more complex architecture and node-wise dynamics.

*Keywords:* discrete dynamics; complex quadratic maps; dynamic networks; low-dimensional directed networks; dynamics.

### 1. Introduction

#### 1.1 Motivation

Many natural systems are organized as self-interacting networks. Subsequently, dynamic networks have been used as a modelling framework in many fields of the life sciences, with definitions of nodes and edges depending on the context. A unifying question for all these different fields regards how the hardwired *structure* of a network (its underlying graph) and its connectivity (edge weights) affect the system's overall *function*. The new term of 'dynamics' has been recently used in reference to investigating simultaneously the network hardwiring (connectomics) and the node-wise temporal evolution (dynamics). The aim is to

understand the contribution of each of these two aspects to the ensemble temporal evolution resulting from their interplay.

The difficulty of the problem did not initially detract from the motivation to address it, a strong drive coming from the potentially tremendous applications to any system in which behaviour emerges from network coupling of interacting nodes. For example, when studying brain networks, the nodes may represent neurons, and the connecting oriented edges between them are synapses with varying weights. In epidemics, the nodes may be populations, and the edges, the physical contacts that promote contagion. For a traffic map, the nodes may be towns, connected by various size roads, and for a social network, individuals are connected by friendship edges of different strengths.

Empirical studies support certain generic topological properties of natural architectures, such as community structure, small-world properties, the existence of hubs and ‘rich clubs’. By applying graph theoretical measures (e.g., clustering coefficient, motifs and modularity), various studies have been investigating the sensitivity of a system’s temporal behaviour to perturbations in the network architecture (e.g., to removing/adding nodes or edges at different places in the network structure). Using graph measures in conjunction with dynamical systems methods originally held great promise towards investigating how the interacting units of a system are wired together and control complex behaviour. In neuroscience, for example, this question is considered one of the great scientific challenges of the 21st century [1–3].

With this aim in mind, a lot of effort was invested in building network models that incorporate graph structure and realistic node-wise dynamics in one unified framework, tractable theoretically or numerically. These can then be used *in conjunction* with data towards interpreting empirical results and for making predictions. Biophysical models revealed rich dynamic regimes and transitions [4], shown to depend as much on the coupling parameters of the network as on the arrangement and strength of its connections, in ways which are difficult to differentiate. While successfully explaining a variety of specific results, biophysical models seem too complex to provide the optimal tools for differentiating between the effects of local dynamics and global architecture, or to be helpful with classifications of dynamics in terms of architectural properties. It has become therefore increasingly clear that, in a naturally realistic setting, this interesting theoretical problem presents potentially insurmountable challenges arising from compounding the graph complexity with the nodes’ dynamic richness.

It has been proposed that simplified, canonical models, while losing the immediate connection with the natural world, may be better suited to identify and pair specific structural patterns with their effects on dynamics. Instead of a focus on rendering specifically the biophysics of any particular natural system, theoretical networks focus (using simpler, lower dimensional graph structures and more tractable, sometimes close to linear, node-wise dynamics) on capturing the phenomenological essence of the question, as well as on establishing methods and results that may work in a more general context. One can then verify whether these methods are more universal, and whether the results can be extended to the more complex networks that describe natural systems.

For example, a standard model historically used to describe and study firing activity in neural populations has been the two-dimensional, nonlinear Wilson-Cowan model [5]. When coupled in even small dimensional networks, Wilson-Cowan equations produce rich behaviour [6]. In our previous work, we developed methods for approaching larger networks with Wilson-Cowan node-wise dynamics, but we observed that analytical and numerical difficulties increase dramatically with size [7]. In order to eliminate some of these issues and keep models analytically tractable for larger sizes, a popular choice has been to ‘linearize’ the Wilson-Cowan system (i.e., approximate a sigmoidal function with three linear pieces [8]).

A newer direction of inquiry initiated by Curto *et al.* [9] is to consider the even simpler node dynamics of threshold-linear networks. The authors study low dimensional networks of simple, perceptron-like

nodes, the difficulty of which is closer to that of linear nodes, but which, when coupled, still exhibit nonlinear-like dynamics due to the way in which the two node-wise linear pieces act on the domain. The authors successfully prove how certain dynamic features (e.g., fixed points and cycles) emerge from the node-wise behaviour in combination with specific network connectivity patterns. Their results support the idea that it is possible, in simple theoretical networks, to infer analytically features of the dynamics from the network's connectivity.

Along the lines of analysing theoretical networks, our study focuses on understanding how architecture affects asymptotic dynamics in networks of complex quadratic maps:  $f_c: \mathbb{C} \rightarrow \mathbb{C}$ ,  $f_c(z) = z^2 + c$ , for  $c \in \mathbb{C}$ . We chose this particular family of node-wise dynamics for three reasons. Firstly, because the node-wise dynamics builds upon over a century of research: the classical theory for single function iterations has been most developed for the complex quadratic family. Secondly, because discrete iterations (and unimodal functions, in particular) have provided good simplified representations for many natural processes such as learning in brain circuits [10–12]. Thirdly, because this is a distinctly different type of dynamics than that considered in the Curto study, which offers a great candidate for testing in the future, whether results are universal (i.e., transcend the type of node-dynamics used for the network). If successful, a long-term goal will be to verify if such results carry over to more complex, physiological node-wise dynamics.

## 1.2 Networks of complex quadratic maps

Work on the complex quadratic family spans more than a century, from the original results of Fatou and Julia, describing in the early 1900s the behaviour of orbits in the dynamic complex plane (reflected by the structure of the Julia set) [13, 14], to bifurcation phenomena in the parameter plane (reflected in the work of Mandelbrot and others, in the 1970s) [15, 16], to recent connections between the two concepts [17–19]. Therefore, we adopted the simplified framework of networked logistic maps as an ideal starting point for approaching basic dynamic questions in the context of networks. In this framework, each network node receives weighted inputs from the adjacent nodes, and integrates these inputs in discrete time as a complex quadratic map. Then the system takes the form of an iteration in  $\mathbb{C}^n$ :

$$z_j(t) \longrightarrow z_j(t+1) = f_j \left( \sum_{k=1}^n g_{jk} A_{jk} z_k \right)$$

where  $n$  is the size of the network,  $A = (A_{jk})_{j,k=1}^n$  is the binary adjacency matrix of the oriented underlying graph, that is  $A_{jk} = 1$  if there is an edge from the node  $k$  to the node  $j$ , and  $A_{jk} = 0$  otherwise. The coefficients  $g_{jk}$  are the signed weights along the adjacency edges (in particular,  $g_{jk} = 0$  if there is no edge connecting  $k$  to  $j$ , that is if  $A_{jk} = 0$ ). In isolation, each node  $z_j(t) \rightarrow z_j(t+1)$ ,  $1 \leq j \leq n$ , iterates as a quadratic function  $f_j(z) = z^2 + c_j$ . When coupled as a network with adjacency  $A$ , each node will act as a quadratic modulation on the sum of the inputs received along the incoming edges (as specified by the values of  $A_{jk}$ , for  $1 \leq k \leq n$ ). In particular, if  $g_{jj} = 0$  (that is if there is no loop from node  $j$  to itself, i.e.,  $A_{jj} = 0$ ), then the node  $j$ 's evolution is based purely on the current state of the other nodes, and not on its own's, which is a situation which is not precluded in natural systems.

We are generally investigating whether one can use properties of multi-dimensional orbits in  $\mathbb{C}^n$ , in particular their asymptotic behaviour (via the topological and fractal structure of Julia and Mandelbrot multi-sets), to classify dynamic behaviour for different network architectures. One may impose additional structural conditions on edge density (i.e., the fraction of oriented edges in the adjacency graph, expressed out of the possible total of  $n^2$ ) or distribution (i.e., the edge configuration in the adjacency graph, for fixed

density). One can then investigate whether it is possible to predict the geometry of Julia and Mandelbrot sets from specific information on the network hardwiring. We aim to tease apart the instances in which small perturbations in the position or strength of one single connection may lead to dramatic topological changes in the asymptotic sets, from the instances in which these sets are robust to much more significant changes.

In our previous work [20], when suggesting possible ties of our results with broader applications to the life sciences, we interpreted iterated orbits as describing the temporal evolution of an evolving system (e.g., learning neural network). An escaping initial condition (whether in the complex plane  $\mathbb{C}$ , for a single iterated map, or in  $\mathbb{C}^n$ , for an iterated network) may be seen as an eventually unsustainable feature of the system, while an initial condition with a bounded forward orbit (a ‘prisoner’) may represent a trivial, or inefficient feature. The Julia set is formed of all the boundary points between prisoners and escapees, hence we suggested that it can be regarded as the ‘critical locus’ of states with a complex temporal evolution, characteristic to living systems operating within an optimal range.

In the same paper [20], we defined the network Mandelbrot set, for simplicity, as the node parameter range for which the critical point (i.e., all nodes equal zero) is bounded (i.e., functionally sustainable) under ensemble iterations of the network. In the traditional case of a single iterated quadratic map, this is equivalent to defining the parameter locus for which the Julia set is connected. Indeed, the Fatou–Julia Theorem delivers in this case a well-known duality: a bounded critical orbit implies a connected Julia set, and an escaping critical orbit implies a totally disconnected Julia set. We do not expect this equivalence to remain true when iterating networks. For networks, we have already noticed that the situation is a lot more complicated: the Julia set may not necessarily be connected or totally disconnected, and may have a finite number of connected components. What we conjectured, in a slightly different form, is that a connected ‘uni-Julia set’ implies a bounded critical orbit, but not conversely.

One may further interpret that, in the case of a network with connected Julia set, all sustainable initial conditions (i.e., prisoners, or initial points leading to bounded orbits) can be reached by perturbations from rest (i.e. from the critical point, with all nodes set at zero), without having to leave the prisoner set. Totally disconnected Julia sets represent a scattered, measure zero locus of sustainable initial states. We further conjectured that one would always have to traverse an intermediate asymptotic region characterized by Julia sets which are disconnected without being totally disconnected, when transitioning from the parameters locus for connected Julia sets to the parameter locus for totally disconnected Julia sets.

### 1.3 *Prior results in small networks*

In order to establish a conceptual framework, in previous work we considered simple, low-dimensional networks, which are both analytically tractable and allow easy visualization and interpretation of the results, suggesting a baseline for extensions to higher dimensional, more complex networks.

We considered in particular three-dimensional networks with various coupling geometries between their complex nodes  $z_1, z_2, z_3$ . For fixed logistic parameters  $c_1=c_2=c_3=c$ , we described the dependence of the Julia and Mandelbrot sets and of their one-dimensional slices on the graph wiring and of the strengths of the connections between nodes.

Our prior work [20] suggests that even basic results from the case of a single iterated quadratic map may have to be rediscovered in the context of networks (one yet needs to prove, for example, even the existence of an escape radius). Although our prior work focused on studying dynamics in small quadratic networks, we had to first give some general definitions for extensions in  $\mathbb{C}^n$  of some of the traditional concepts: multi-orbits, Julia and Mandelbrot sets, as well as their one-dimensional complex slices, which

we called uni-Julia and equi-Mandelbrot sets. For completeness purposes, these definitions are reproduced below:

**DEFINITION 1.1** For a fixed parameter  $(c_1, \dots, c_n) \in \mathbb{C}^n$ , we call the **prisoner set** of the network, the locus of  $(z_1, \dots, z_n) \in \mathbb{C}^n$  which produce a bounded multi-orbit in  $\mathbb{C}^n$ . We call the **uni-prisoner set**, the locus of  $z \in \mathbb{C}$  so that  $(z, \dots, z) \in \mathbb{C}^n$  produces a bounded multi-orbit. The **multi-Julia set (or the multi-J set)** of the network is defined as the boundary in of the multi-prisoner set (as a subset in  $\mathbb{C}^n$ , with the product topology). Similarly, one defines the **uni-Julia set (or uni-J set)** of the network as the boundary in  $\mathbb{C}$  of the uni-prisoner set for that network.

**DEFINITION 1.2** We define the **multi-Mandelbrot set (or the multi-M set)** of the network the parameter locus of  $(c_1, \dots, c_n) \in \mathbb{C}^n$  for which the multi-orbit of the critical point  $(0, \dots, 0)$  is bounded in  $\mathbb{C}^n$ . We call the **equi-Mandelbrot set (or the equi-M set)** of the network, the locus of  $c \in \mathbb{C}$  for which the critical multi-orbit is bounded for **equi-parameter**  $(c_1, c_2, \dots, c_n) = (c, c, \dots, c) \in \mathbb{C}^n$ . We call the  **$k$ th node-wise equi-M set** the locus  $c \in \mathbb{C}$  such that the  $k$ th component of the multi-orbit of  $(0, \dots, 0) \in \mathbb{C}^n$  remains bounded in  $\mathbb{C}$ .

In our previous article, we applied these definitions to a variety of three-dimensional systems and we pointed out new, network phenomena. We proposed new versions of the traditional theorems for the case of networked nodes. We showed that even in networks where all nodes have the same parameter  $c$  (i.e., the same quadratic map is used for all components in  $\mathbb{C}^n$ ), their behaviour may not be ‘synchronized’, in the sense that different nodes may have different asymptotic behaviour (reflected in differences between node-wise Mandelbrot and Julia sets). Node coupling seems to enhance this ‘de-synchronization’ between two or more nodes, and additional networking may generally lead to smaller network Mandelbrot and Julia sets. Unlike for the traditional single map iterations, the definition requirement for the M-set that the origin has a bounded multi-orbit is no longer equivalent with that of the J-set being connected, in either of its forms (multi-J or uni-J set). In our previous work, however, we have conjectured a weaker version of the Fatou–Julia theorem in this case, which remains to be verified analytically. We also analysed and interpreted the distinct effects of varying the signed connection strengths, and those of introducing feedback into the network.

We finally pointed out that complex natural networks are typically a lot larger than the three and four node networks we had studied. At the same time, however, natural networks (such as brain circuits, for example) tend to be highly hierarchic, with the behaviour of each one node at a certain complexity level integrating the behaviour of a collection of lower-level nodes. Hence, at each complexity level, the size of the network to be studied may be in fact relatively small (tens or hundreds of nodes). While for small networks the effects of architecture on asymptotic dynamics can still be observed and studied by looking at each configuration individually, and for very large networks one may take the large size limit approach traditional in random graph theory, for these intermediate networks one has to build different approaches, which we further explore here.

Within this article, we will focus on studying equi-M and uni-J sets for networks with identical nodes (i.e., network dynamics for equi-parameters  $c \in \mathbb{C}$ ). The article is organized as follows. In Section 2, we state sufficient conditions for existence of an escape radius. Under these conditions, we calculate the radius in terms of the network parameters. In Sections 2.2 and 2.3, we consider a particular three-dimensional model, and for this model we explore under what conditions (i.e., for which network configuration and edge weights) the network Mandelbrot set preserves the connectivity and the hyperbolic bulb structure

that are its signature in the case of single map iterations. In Section 2.4, we investigate, for the same low-dimensional example model, a form of the Fatou–Julia Theorem for networks. We test whether the uni-Julia set connectedness locus coincides with the post-critically bounded locus, both considered as subsets in the space of edge weights. Since the result does not hold in a similar form to the original theorem for single iterated maps, we use numerical computations to conjecture an extension. In Section 3, we introduce new methods applicable to higher dimensional networks. We investigate the robustness of the asymptotic sets under changes in the graph structure, and investigate whether one can use the network Mandelbrot set to define classes of asymptotic dynamics within the set of dynamic networks with  $n$  nodes and all possible edge configurations. We introduce a statistical book-keeping method developed in our previous work [7] to define probabilistic (or average) versions of the Julia and Mandelbrot sets, illustrating the likelihood that each initial state of the network remains bounded when iterated under a random network configuration with certain given properties. Using this framework, one can attempt to tease apart graph theoretical features determinant of certain dynamics of the network, from those less consequential to temporal behaviour. Finally, in Section 4, we interpret our results and comment on potential applications.

## 2. Extensions of traditional results

### 2.1 Escape radius

A simple and well-known result in the case of single quadratic map iterations is the existence of escape radius [21]. More precisely:

**THEOREM 2.1** For any value of the parameter  $c \in \mathbb{C}$ , the function  $f_c(z) = z^2 + c$  has the escape radius  $R_e = \max(|c|, 2)$ . That is: for any arbitrary orbit  $z(n)$ , with  $n \geq 0$ , if the  $N$ th iterate  $|z(N)| > R_e$  for some  $N \geq 0$ , then  $|z(n)| > R_e$  for all  $n \geq N$ , and  $|z(n)| \rightarrow \infty$  as  $n \rightarrow \infty$ .

*Proof.* Suppose  $|z(n)| > R_e$  for some  $n \geq N$  and calculate:

$$\frac{|z(n+1)|}{|z(n)|} = \frac{|f_c(z(n))|}{|z(n)|} = \frac{|z(n)^2 + c|}{|z(n)|} \geq \frac{|z(n)|^2 - |c|}{|z(n)|} = |z(n)| - \frac{|c|}{|z(n)|}$$

Since  $|z(n)| > |c|$ , it follows that  $\frac{|z(n+1)|}{|z(n)|} \geq |z(n)| - 1$ . We also have that  $|z(n)| > 2$ , hence it follows that  $|z(n+1)| > |z(n)|$ . If we assume  $|z(N)| > \max(|c|, 2)$ , the conclusion of the theorem follows easily by induction.  $\square$

We are interested in finding whether/when this is also the case for networks. What we mean by a network  $\mathcal{N}$  having the escape radius property is the following:

**DEFINITION 2.2** Consider a network  $\mathcal{N} = (z_i)_{i=1}^n$ , with coupled complex dynamics on its nodes, and define the norm of the network as  $\|z(k)\|^2 = \sum_{i=1}^n |z_i(k)|^2$ , at each iteration step  $k \geq 0$ . We say that  $\mathcal{N}$  has the **escape radius property** if there exists a large enough  $R > 0$  such that if  $\|z(K)\| > R$  at some iterate  $K \geq 0$ , then  $\|z(k)\| > R$  for all  $k > K$ , and  $\|z(k)\| \rightarrow \infty$  as  $k \rightarrow \infty$ .

We expect the answer to vary with the network, so that both existence and size of the escape radius would depend on the network's architecture and edge weights. While in general it would be desirable

to find equivalent conditions for a network to have the escape radius property, here we describe two sufficient conditions (two relatively broad classes of networks which cover our subsequent numerical investigations).

**DEFINITION 2.3** Let  $\mathcal{N}$  be a network with  $n$  nodes, with the edge connecting the node  $j$  to the node  $i$  having weight  $g_{ij}$  (for all  $1 \leq i, j \leq n$ , where  $g_{ij} = 0$  when there is no edge connecting the nodes). Suppose that these weights are so that, for each node  $1 \leq j \leq n$ , there exists a node  $\sigma(j)$  for which

$$|g_{\sigma(j)j}| > \sum_{l \neq j} |g_{\sigma(j)l}|$$

In other words, each node sends to another node of its choice a projection edge, which is stronger in absolute value than the sum of the absolute values of the strengths along all other incoming edges to the receiving node. Then we say that  $\mathcal{N}$  is a **dominated** network.

**THEOREM 2.4** Dominated networks with identical  $c$  values for all nodes have escape radius.

*Proof.* We will show that there exists  $\delta > 1$  and  $M_0 > 0$  such that, for all  $M \geq M_0$  and all  $K \geq 0$ , if

$$|z_i(k)| \leq M, \text{ for all nodes } 1 \leq i \leq n \text{ and all iterates } 0 \leq k \leq K + 1 \quad (1)$$

then

$$|z_i(k)| \leq \frac{M}{\delta}, \text{ for all nodes } 1 \leq i \leq n \text{ and iterates } 0 \leq k \leq K \quad (2)$$

This implies that, if  $|z_i(k)| > M/\delta$  for some node  $1 \leq i \leq n$  and some iterate  $k \geq 0$ , then there exists a node  $1 \leq l \leq n$  for which  $|z_l(k+1)| > M$ . In other words, we show that once a node gets large enough in modulus, at each future iteration step one of the nodes (not necessarily the same one each time) will be even larger, causing the norm to escape to infinity. This is equivalent to the definition of the escape radius property, as previously stated.

Indeed, suppose we have (1) for some  $M > 0$ . We want to see what conditions  $M$  needs to meet in order to satisfy (2). Fix an arbitrary node  $1 \leq j \leq n$ . Since the network is dominated, there will exist a node  $\sigma(j)$  such that  $|g_{\sigma(j)j}| > \sum_{l \neq j} |g_{\sigma(j)l}|$ . Then:

$$|z_{\sigma(j)}(K+1)| = \left| \left[ \sum_l g_{\sigma(j)l} z_l(K) \right]^2 + c \right| \geq \left| \sum_l g_{\sigma(j)l} z_l(K) \right|^2 - |c|$$

Hence

$$\left| \sum_l g_{\sigma(j)l} z_l(K) \right| \leq \sqrt{|z_{\sigma(j)}(K+1)| + |c|}$$

and

$$|g_{\sigma(j)j} z_j(K)| \leq \sqrt{|z_{\sigma(j)}(K+1)| + |c|} + \left| \sum_{l \neq j} g_{\sigma(j)l} z_l(K) \right|$$

Using (1), it follows that:

$$|g_{\sigma(j)}z_j(K)| \leq \sqrt{M + |c|} + M \left| \sum_{l \neq j} g_{\sigma(j)l} \right|$$

If we required that the right side be smaller than  $\frac{M}{\delta}|g_{\sigma(j)}|$ , it would follow automatically that  $|z_j(K)| \leq M/\delta$ . We want to find out whether we can choose  $M$  so that this stricter condition is satisfied:

$$\begin{aligned} \sqrt{M + |c|} + M \left| \sum_{l \neq j} g_{\sigma(j)l} \right| &\leq \frac{M}{\delta} |g_{\sigma(j)}| \iff \\ \sqrt{M + |c|} &\leq \frac{M}{\delta} \left( |g_{\sigma(j)}| - \delta \left| \sum_{l \neq j} g_{\sigma(j)l} \right| \right) \end{aligned}$$

Since  $|g_{\sigma(j)}| > \sum_{l \neq j} |g_{\sigma(j)l}|$ , there exists  $M_0^{(j)} > 0$  and  $\delta^{(j)} > 1$  such that the inequality is satisfied for any  $M > M_0^{(j)}$  and  $\delta < \delta^{(j)}$ .

Since this is true for any arbitrary  $1 \leq j \leq n$ , we can define  $M_0 = \max_j M_0^{(j)}$ . Then (2) is satisfied for any  $M \geq M_0$ , for  $\delta = \min_j \delta^{(j)}$ . This concludes the proof.  $\square$

**DEFINITION 2.5** We say that a network is feed-forward with self loops if  $g_{ii} \neq 0$  for all  $1 \leq i \leq n$ , and if for all nodes  $1 \leq j \leq n$  and all iterations  $k \geq 0$  we have

$$z_j(k+1) = \left[ \sum_{l \leq j} g_{jl} z_l(k) \right]^2 + c$$

(in other words, if its adjacency matrix is lower triangular and has no diagonal zeros).

**Remark.** A network is feed-forward with self loops if each node is only coupled with its predecessors and with itself. Notice that in this case the adjacency matrix is nonsingular. All the networks considered in our numerical experiments in the rest of this article are feed-forward with self loops. Studying dynamics in feed-forward networks may present additional interest, since it may relate to existing work on skew products in  $\mathbb{C}^n$  [22–25].

**THEOREM 2.6** Feed-forward networks with self loops and identical  $c$  values for all nodes have the escape radius property.

*Proof.* Fix  $\delta > 1$ . We will show that there exists  $M_0 > 0$  such that for all  $M > M_0$ , if  $|z_j(k)| \geq M$  for some  $1 \leq j \leq n$  and some  $k \geq 0$ , then  $|z_l(k+1)| \geq \delta M$ , for some  $1 \leq l \leq n$ . This implies that if one node gets larger in modulus than  $M_0$  at some stage  $k$  of the iteration, then  $\|z(k)\| \rightarrow \infty$  as  $k \rightarrow \infty$ . In other words,  $M_0$  would act as an escape radius for the network.

We will prove this by induction over the network size  $n$ . For the first node  $z_1$ , the result is equivalent to the existence of escape radius for a single quadratic map (hence we can take  $M_0^{(1)} = \max(|c|, 2)$ , according to Theorem 2.1).

Suppose that the result holds for the feed-forward network consisting of the first  $(n - 1)$  nodes, for some  $M_0^{(n-1)}$ . That is: for all  $M > M_0^{(n-1)}$ , if  $|z_j(k)| \geq M$  for some  $1 \leq j \leq n - 1$  and some  $k \geq 0$ , then  $|z_l(k + 1)| \geq \delta M$ , for some  $1 \leq l \leq n - 1$ . We will show that it holds for the feed-forward network of  $n$  nodes with self loops, for an  $M_0^{(n)}$  large enough. More precisely, as it will become apparent along the rest of the proof, it is sufficient to make a choice that satisfies the following conditions:

- (i)  $M_0^{(n)} > M_0^{(n-1)}$
- (ii)  $M_0^{(n)} > M_0^{(n-1)} \frac{\sum_{l < n} |g_{nl}|}{|g_{nn}|}$  (the right hand is finite because  $|g_{nn}| \neq 0$  for all  $n$ )
- (iii)  $\left( M |g_{nn}| - M_0^{(n-1)} \sum_{l < n} |g_{nl}| \right)^2 > |c|M$

Since the last condition is satisfied by  $M_0^{(n)}$  being larger than the larger root  $M_+$  of the quadratic equation

$\left( M |g_{nn}| - M_0^{(n-1)} \sum_{l < n} |g_{nl}| \right)^2 - |c|M = 0$ , a sufficient condition for  $M_0^{(n)}$  is that

$$M_0^{(n)} > \max \left( M_0^{(n-1)}, M_0^{(n-1)} \frac{\sum_{l < n} |g_{nl}|}{|g_{nn}|}, M_+ \right) \quad (3)$$

Consider an  $M_0^{(n)}$  satisfying property (3). Fix an arbitrary  $M > M_0^{(n)}$ , and suppose we have  $|z_l(k)| \geq M \geq M_0^{(n)}$ , for some  $1 \leq l \leq n$  and some  $k \geq 0$ . We have two cases:

*Case 1.* If  $|z_j(k)| \geq M$  for some  $1 \leq j \leq n - 1$  and the  $k$  in the hypothesis above. Then, since  $M \geq M_0^{(n)} > M_0^{(n-1)}$ , we can use the result from the  $n - 1$  induction step, and get that  $|z_l(k + 1)| \geq \delta M$ , for some  $1 \leq l \leq n - 1$ .

*Case 2.* If  $|z_j(k)| < M$  for all  $1 \leq j \leq n - 1$ , then it must be that  $|z_n(k)| \geq M$ .

Since the iteration in the  $n$ th node is given by:

$$z_n(k + 1) = \left( \sum_l g_{nl} z_l(k) \right)^2 + c$$

we can use the triangle inequality to get

$$|z_n(k + 1)| \geq \left| \sum_l g_{nl} z_l(k) \right|^2 - |c|$$

Hence

$$\begin{aligned} \sqrt{|z_n(k+1)| + |c|} &\geq \left| \sum_l g_{nl} z_l(k) \right| \geq |g_{nn}| \cdot |z_n(k)| - \sum_{l < n} |g_{nl}| \cdot |z_l(k)| \\ &\geq M |g_{nn}| - M_0^{(n-1)} \sum_{l < n} |g_{nl}| \end{aligned}$$

Since the right side of the inequality is positive (from requirement (ii) on  $M_0^{(n)}$ ), the condition is then equivalent with:

$$|z_n(k+1)| \geq \left( M |g_{nn}| - M_0^{(n-1)} \sum_{l < n} |g_{nl}| \right)^2 - |c|$$

From requirement (iii) on  $M_0^{(n)}$ , it follows that  $|z_n(k+1)| \geq \delta M$ .

In conclusion, in both cases it follows that  $|z_l(k+1)| \geq \delta M$  for some  $1 \leq l \leq n$ , which concludes the induction. □

### 2.2 Main cardioid and periodic bulbs

Possibly, the most striking geometric features of the traditional Mandelbrot set are its periodic Fatou components. Indeed, one may consider the set  $\mathcal{M}'$  of all parameters  $c$  for which the map  $f_c$  has an attracting periodic orbit. It has been established that  $\mathcal{M}'$  is a subset of the interior of  $\mathcal{M}$ . For example, the  $c$ -locus for which the map has an attracting fixed point represents the interior of the main cardioid of  $\mathcal{M}$ , and the locus for which the map has an attracting period two orbit is the interior of the disc of radius  $1/4$  centred at  $(-1, 0)$ . Whether  $\mathcal{M}'$  is in fact identical to the interior of  $\mathcal{M}$ , or  $\mathcal{M}$  contains other ('ghost', persistently non-hyperbolic [26]) interior points—is still an open question, known as the Density of Hyperbolicity conjecture. While the conjecture was solved for real polynomials over twenty years ago [27, 28], it still represents one of the most important open problems in complex dynamics.

In the traditional case of single iterated maps, each hyperbolic component (bulb) of the Mandelbrot set represents a parameter subset for which the map has an attracting orbit of period  $k$ . For example, the locus in  $\mathbb{C}$  for which the map has an attracting fixed point is the interior of the main cardioid, defined as

$$c = \frac{e^{i\theta}}{2} - \frac{e^{2i\theta}}{4}, \text{ with } 0 \leq \theta \leq 2\pi.$$

We ask whether one may be able to define (and set to compute in a similar fashion) hyperbolic components for a network of quadratic complex nodes. To fix our ideas, we aim to calculate the main hyperbolic component (representing the locus of  $c \in \mathbb{C}$  for which the network has an attracting fixed point) for a very simple network of three nodes (which we had considered in previous work). We will illustrate how the boundary of this region differs from the main cardioid from the traditional case, and compare it with the numerical illustrations of the corresponding equi- $M$  sets.

Consider the following 'simple dual' network with two input nodes and one output node (as considered in our previous work [20]):

$$\begin{aligned} z_1 &\rightarrow z_1^2 + c \\ z_2 &\rightarrow (az_1 + z_2)^2 + c \\ z_3 &\rightarrow (z_1 + z_2)^2 + c \end{aligned}$$

where  $a$  is the level of cross-talk between the input nodes. We ask that  $(z_1, z_2, z_3)$  be a fixed point:  $z_1^2 + c = z_1$  (with roots  $z_1^{(1)}$  and  $z_1^{(2)}$ ) and  $(az_1 + z_2)^2 + c = z_2$  (producing two roots  $z_2^{(1,1)}$  and  $z_2^{(1,2)}$  corresponding to  $z_1 = z_1^{(1)}$ , and two roots  $z_2^{(2,1)}$  and  $z_2^{(2,2)}$  corresponding to  $z_1 = z_1^{(2)}$ ). Hence, there are in general four fixed points for the subnetwork formed of the first two nodes, namely:  $(z_1^{(1)}, z_2^{(1,1)})$ ,  $(z_1^{(1)}, z_2^{(1,2)})$ ,  $(z_1^{(2)}, z_2^{(2,1)})$  and  $(z_1^{(2)}, z_2^{(2,2)})$ . With this, the third component  $z_3 = (z_1 + z_2)^2 + c$  is fixed automatically (since it is independent of  $z_3$ ), producing four corresponding fixed points for the original three-dimensional network, which we will call  $z_{1,1}^*$ ,  $z_{1,2}^*$ ,  $z_{2,1}^*$  and  $z_{2,2}^*$ . The Jacobian matrix of this network

$$J(z_1, z_2, z_3) = \begin{pmatrix} 2z_1 & 0 & 0 \\ 2a(az_1 + z_2) & 2(az_1 + z_2) & 0 \\ 2(z_1 + z_2) & 2(z_1 + z_2) & 0 \end{pmatrix} \quad (4)$$

has eigenvalues  $\lambda_1 = 2z_1$ ,  $\lambda_2 = 2(az_1 + z_2)$  and  $\lambda_3 = 0$  (super-attracting component). To find the boundary of the hyperbolic component, we calculate the curve  $|\lambda_1| = |\lambda_2| = 1$  at each of the fixed points, separating the region where these fixed points are stable (attracting) from the region where they have unstable (saddle) behaviour. For simplicity, call  $\varphi = az_1 + z_2$ , and notice that the eigenvalue condition implies  $2z_1 = e^{i\theta}$ , with  $0 \leq \theta \leq 2\pi$ , and  $2\varphi = e^{i\tau}$ , with  $0 \leq \tau \leq 2\pi$ .

The first condition implies that  $c = z_1 - z_1^2 = \frac{e^{i\theta}}{2} - \frac{e^{2i\theta}}{4}$ , which is precisely the main cardioid from the traditional case. The second condition will add another restriction, which will depend on parameter  $a$ . It follows immediately, however, that the network hyperbolic component will always be a subset of the interior of the main cardioid from the traditional case of single map iterations.

Notice now that the first fixed point equation multiplied by  $a$  and added to the second delivers:  $az_1^2 = \varphi - \varphi^2 - (a+1)c$ , while the second gives us:  $\varphi^2 + c = \varphi - az_1$ , hence  $az_1 = \varphi - \varphi^2 - c$ . In conclusion:

$$a^2 z_1^2 = a\varphi - a\varphi^2 - a(a+1)c = (\varphi - \varphi^2 - c)^2$$

Calling  $\xi = \varphi - \varphi^2$ , we obtain the quadratic equation in  $c$ :

$$c^2 + (a^2 + a - 2\xi)c + \xi^2 - a\xi = 0$$

which gives the solution curves:

$$\begin{aligned} c &= \frac{2\xi - a - a^2 \pm \sqrt{a^2(a+1)^2 - 4a^2\xi}}{2} \\ &= \frac{2(\varphi - \varphi^2) - a - a^2 \pm \sqrt{a^2(a+1)^2 - 4a^2(\varphi - \varphi^2)}}{2} \end{aligned}$$

where  $\varphi = e^{i\tau}/2$ . We represented these curves and the regions between them in Fig. 1.

Notice that having an attracting fixed point for the network no longer implies that the origin will be in the attraction basin of this fixed point, hence the critical orbit can still escape (as shown in Fig. 1). Hence even in networks as simple as this family of examples, structuring the interior of M-set as a union of hyperbolic bulbs fails. While some of the bulb geometry is preserved (e.g., the cusp seems robust under network transformations), some of the landmarks lose their dynamic context (e.g. the origin  $c = 0$ , while still in the network Mandelbrot set, can no longer be regarded as the centre of a main cardioid).

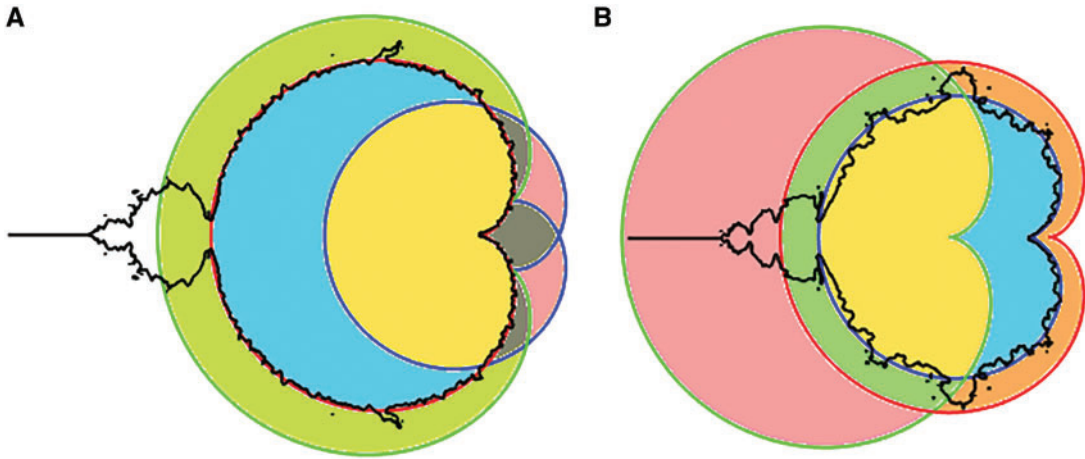


FIG. 1. Main hyperbolic component of the network equi-M set, for a simple dual network with different cross-talk values  $a$  (see the main text for the node-wise iterations corresponding to this model). The panels show the boundary of the equi-M set (computed numerically) and the curves obtained analytically, for two different values of the parameter  $a$ : (A)  $a = -1/3$  and (B)  $a = 1/3$ . The red curve represents the traditional Mandelbrot cardioid, and the green and blue curves represent the additional restriction curves for  $c$ , as described in the text. With the notation for the four fixed points  $z_{1,1}^*$ ,  $z_{1,2}^*$ ,  $z_{2,1}^*$  and  $z_{2,2}^*$  introduced in the main text, the colours represent different stability behaviours of the critical components, as follows: in the olive region,  $|\lambda_2| < 1$  at  $z_{1,1}^*$ ; in the blue regions, both  $|\lambda_1| < 1$  and  $|\lambda_2| < 1$  at  $z_{1,1}^*$  and  $|\lambda_2| < 1$  at  $z_{2,1}^*$ ; in the yellow regions, both  $|\lambda_1| < 1$  and  $|\lambda_2| < 1$  at  $z_{1,1}^*$  and  $|\lambda_2| < 1$  at  $z_{2,1}^*$ ; in the gray regions,  $|\lambda_2| < 1$  at  $z_{1,1}^*$  and  $z_{2,1}^*$ ; in the pink regions,  $|\lambda_2| < 1$  at  $z_{2,1}^*$ ; in the green region,  $|\lambda_2| < 1$  at  $z_{1,2}^*$  and  $z_{2,2}^*$ ; in the orange region,  $|\lambda_1| < 1$  at  $z_{1,1}^*$ . In conclusion, the network has an attracting fixed point within the union of the yellow and blue regions.

The properties of higher period bulbs get perturbed even more dramatically. We can track, for example, what becomes of the period two bulb/disc (originally centred at the  $c = -1$ ) in the two parameter family of simple three-dimensional networks given by  $z_1 \rightarrow z_1^2 + c$ ,  $z_2 \rightarrow (az_1 + z_2)^2 + c$ ,  $z_3 \rightarrow (z_1 + z_2 + bz_3)^2 + c$ , with  $a, b \in \mathbb{R}$ . While part of the topological behaviour of the original Mandelbrot set is conserved in some networks, it completely collapses in others, depending on the configuration and connectivity parameters. To illustrate, we first show in Fig. 2 a comparison between the network Mandelbrot sets for our model network, for three different parameter pairs:  $(a, b) = (-1, -1)$ ;  $(a, b) = (-1/3, -1/3)$  and  $(a, b) = (-2/3, -1/3)$ . In all cases, the M-set is disconnected (see Section 2.3 for detail); in the first two cases,  $c = -1$  is still part of the set; in the third, it is not.

### 2.3 Connectedness of the Mandelbrot set

A set in  $\mathbb{C}$  is said to be disconnected if it is a subset of the disjoint union of two open sets, both of which it intersects. A set is connected if it is not disconnected. Establishing connectedness of the traditional Mandelbrot set has been historically challenging, with an original conjecture (based on numerical and visual consideration) stating the exact opposite. Connectedness of the set was finally determined by Douady and Hubbard [29], with a proof based on the construction of a conformal isomorphism between the complement of the Mandelbrot set and the complement of the closed unit disk.

It has been hypothesized that the Mandelbrot set is locally connected (the MLC conjecture). While local connectivity has been established at many special points in the Mandelbrot set (for example, Yoccoz proved that this is the case at all finitely renormalizable parameters [30]), the general conjecture remains

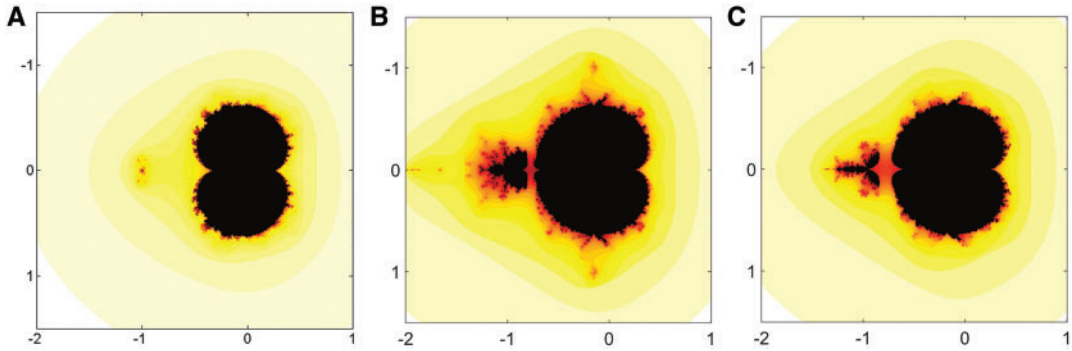


FIG. 2. Examples of disconnected equi-M sets for two networks with  $N = 3$  nodes. All three networks belong to the family:  $z_1 \rightarrow z_1^2 + c$ ,  $z_2 \rightarrow (az_1 + z_2)^2 + c$ ,  $z_3 \rightarrow (z_1 + z_2 + bz_3)^2 + c$ . (A) Connectivity weights  $a = -1$ ,  $b = -1$ ; (B) Connectivity weights  $a = -1/3$ ,  $b = -1/3$ ; (C) Connectivity weights  $a = -2/3$ ,  $b = -1/3$ . The colours represent the escape rate of the critical orbit out of the disc of radius  $R_c = 20$ , so that the critical orbit is bounded in the central black region, and escapes faster with increasingly lighter colours.

open. Establishing local connectedness of the Mandelbrot set is extremely desirable, since it implies Density of Hyperbolicity [29].

It is not entirely surprising that most of these results no longer apply in this form for networked complex maps. For example, connectedness fails in general for network equi-Mandelbrot sets. To fix our ideas, we illustrate and prove disconnectedness for an example network in the three-dimensional family considered previously [20] (see Fig. 2). This family (which we called the ‘self-drive model’) is interesting and easy to analyse, since each node depends only on the ones with smaller indices:  $z_1 \rightarrow z_1^2 + c$ ,  $z_2 \rightarrow (az_1 + z_2)^2 + c$ ,  $z_3 \rightarrow (z_1 + z_2 + bz_3)^2 + c$  (i.e., this is a family of feed-forward networks, having from one to three self loops, since  $a$  and  $b$  are allowed to be zero).

**PROPOSITION 2.7** The equi-M set for the network in the self-drive family (equations described above) with connectivity weights  $a = -1$ ,  $b = -1$  is disconnected.

*Proof.* Notice first that, in general, all three node-wise projections of the critical orbits are real. We will show that the equi-M set described in the proposition has at least two connected components (the component of the origin and that of  $c = -1$ ), separated by the line  $\text{Re}(z) = -3/4$  (see Fig. 3).

Indeed, the critical orbit is fixed for  $c = 0$ , so that  $c = 0$  is trivially in the equi-M set of the network. Also, one can easily see that this particular self-drive network is post-critically finite when  $c = -1$ . Indeed, the first component of the critical orbit has in this case period two ( $0 \rightarrow -1$ ); the second component has period four ( $0 \rightarrow -1 \rightarrow -1 \rightarrow 0$ ) and the third component has period four ( $0 \rightarrow -1 \rightarrow 0 \rightarrow 0$ ).

Finally, one can easily prove that no point on the line  $\text{Re}(c) = -3/4$  is in the equi-M set of this network. Indeed, notice that  $c = -3/4$  is the only point in the traditional Mandelbrot set with  $\text{Re}(c) = -3/4$  (it is the point joining the main cardioid and the period two bulb). Since the network M-set is a subset of the node-wise M-set for  $z_1$  (which is the traditional Mandelbrot set), it also cannot contain any other points with  $\text{Re}(c) = -3/4$ . Furthermore, for our network, it can be shown that the third component  $z_3$  of the critical orbit escapes when  $c = -3/4$ . Hence no point on the vertical line  $c = -3/4$  is in the equi-M set of the network. It is interesting that the node that causes the pinch in the traditional M-set and renders the

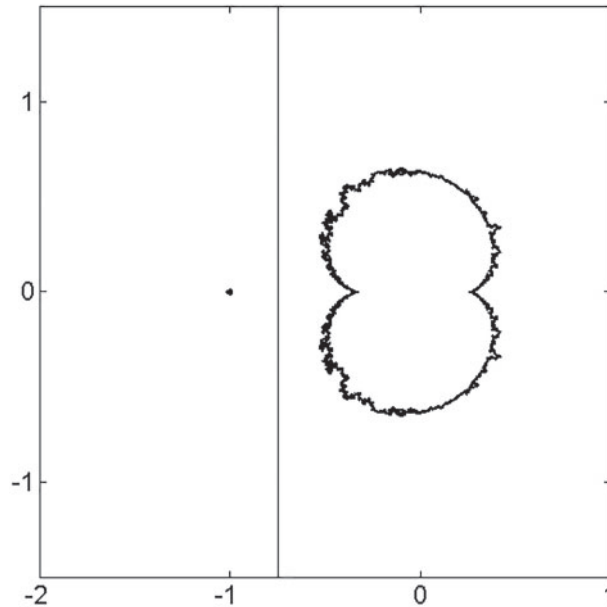


FIG. 3. Example of disconnected equi-M set for a network with  $N = 3$  nodes. The curve traces the boundary of the equi-M set shown in Fig. 2a, separated into two connected components, separated by the line  $Re(z) = -3/4$ : the one containing  $c = 0$ , to the right of the line, and the one containing  $c = -1$ , to the left of the line. The network is given by  $z_1 \rightarrow z_1^2 + c$ ,  $z_2 \rightarrow (az_1 + z_2)^2 + c$ ,  $z_3 \rightarrow (z_1 + z_2 + bz_3)^2 + c$ , with connectivity weights  $a = -1$ ,  $b = -1$ .

network M-set disconnected is in fact the ‘output’ node, which receives control from both of the other two nodes; yet it is the orbit of  $z_3$  that escapes, while the other two remain bounded when initiated at zero. Since the calculations are a little technical, we include them for completion in Appendix A.  $\square$

More generally, one can take advantage of the fact that values of  $c$  on the real axis deliver real critical orbits in combination with the real coupling strengths, hence one can use real map iterations and bifurcation diagrams to understand the conditions for super-attracting, or for post-critically bounded networks in the self-drive network model. Below, we carry out an example of such a bifurcation analysis with respect to the coupling parameters  $a$  and  $b$ , for the special case of fixed  $c = -1$ . This is a point where computations are relatively simple, since it represents a parameter value for which the critical point of the traditional quadratic map has period two. We are additionally interested in this special case, since we want to investigate the potential relationship between the combinatorics at the former hyperbolic bulb centres and the connectivity of the equi-M set. Since  $c = -1$  is the simplest nontrivial centre, this discussion represents a first step towards this goal.

Fix  $c = -1$  and  $a = -1$ , keeping the critical orbits of the first two nodes periodic ( $z_1$  performs a period two oscillation between  $0 \rightarrow -1$ , and  $z_2$  has a period four oscillation  $0 \rightarrow -1 \rightarrow -1 \rightarrow 0$ ), and study the effect of changing the self-drive parameter  $b$  on the critical orbit of the node  $z_3$ . The bifurcation diagram in Fig. 4 illustrates that in the parameter slice  $a = -1$ , there are at least three intervals for  $b$  for which  $c = -1$  is in the equi-M set.

These intervals include the windows corresponding to attracting fixed points, but also encompass period-doubling cascades and chaotic windows (not shown in Fig. 4). Given with three decimal places

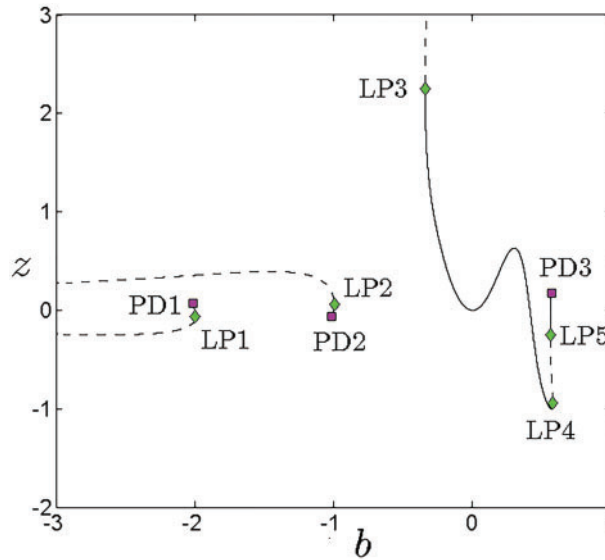


FIG. 4. Bifurcation diagram with respect to the coupling parameter  $b$  for the function  $f(\xi) = f_4 \circ f_3 \circ f_2 \circ f_1(\xi)$ , which computes every fourth iteration of the node  $z_3$ , when  $a = -1$ , so that  $f_1(\xi) = b^2\xi^2 - 1$ ,  $f_2(\xi) = (b\xi - 2)^2 - 1$ ,  $f_3(\xi) = (b\xi - 1)^2 - 1$  and  $f_4(\xi) = f_3(\xi)$ . The diagram shows three equilibrium curves, with a green diamond marking saddle node bifurcations (limit points/LP), and purple squares marking the first period doubling point of period doubling cascades to chaos. Stable equilibria are shown as solid lines, and unstable equilibria are shown as dotted lines. The intervals on which there is a stable equilibrium are  $b \sim -2.001$  (PD1) to  $b \sim -1.995$  (LP1);  $b \sim -1.01$  (PD2) to  $b \sim -0.996$  (LP2);  $b \sim -0.34$  (LP3) to  $b \sim 0.58$  (LP4), with a second stable fixed point between  $b \sim 0.56$  (LP5) and  $b \sim 0.57$  (PD3). The subsequent period doubling and chaotic windows are not shown, for clarity of the diagram (since two of these windows are extremely small), but the critical orbit remains bounded within this extended parameter range (as mentioned in the text). The diagram was created using the MatContM software for continuation and bifurcations in discrete map iterations [31], implemented in Matlab, with double precision.

of approximation, these intervals for the parameter  $b$  are:  $[-2.016, -1.995]$ ,  $[-1.028, -0.996]$  and  $[-0.34, 0.611]$ .

Even more generally, one can compute the range for the coupling parameter  $a$  which guarantees that  $c = -1$  remains in the node-wise Mandelbrot set for the second node  $z_2$ . Since the critical orbit is real for real values of  $c$  and  $a$ , we can study this by tracking the bifurcations of the function  $f(\xi) = (\xi^2 - 1 - a)^2 - 1$  (which represents the transition between even iterations of  $z_2$ ) with respect to  $a$ . We show the bifurcation diagram schematically in Fig. 5. The initial condition  $z_2(0) = 0$  escapes for  $a < -2$ ; it converges to a stable fixed point starting at  $a = -2$ , and then to a stable period two orbit (after the period doubling at  $a = -5/4$ ). The attracting period two orbit survives (and attracts the origin) until  $a = -0.4$  (with a superattracting stage at  $a = -1$ ), and then collapses back into a stable fixed point. As  $a$  is increased, the system undergoes a cascade of period doubling bifurcations, starting with the first one at  $a \sim 0.15$ , birthing periodic cycles which continue to attract the critical orbit; this continues along on the route to chaos, maintaining  $z_2$  bounded. Eventually, the origin escapes the trapping interval when the parameter crosses the value  $a \sim 0.7$ .

Hence  $c = -1$  is in the  $z_2$  Mandelbrot set for the relatively large interval  $[-2, 0.7]$  for  $a$ , and is not in the node-wise Mandelbrot set outside this parameter range. The two endpoints of this interval have different significance and mechanisms. On one hand, when lowering  $a$  past the low critical state  $a = -2$ , the point  $c = -1$  pinches out and separates the  $z_2$  Mandelbrot set into two connected components (to

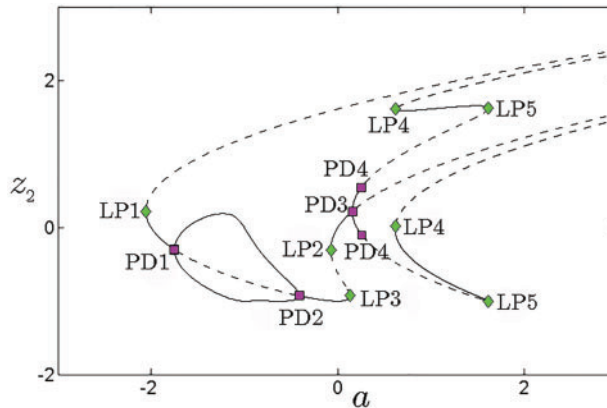


FIG. 5. Bifurcation diagram with respect to the coupling parameter  $a$  for the function  $f(\xi) = (\xi^2 - 1 - a)^2 - 1$  (representing the even iterations of the  $z_2$  component of the critical orbit in the feed-forward family when  $c = -1$ ). The diagram shows equilibrium curves, with a green diamond marking saddle node bifurcations (limit points/LP), and purple squares marking the first and second period doubling points in the cascades to chaos. The subsequent period doubling and chaotic windows are not shown, for clarity of the diagram. Stable equilibria and periodic orbits are shown as solid lines, and unstable equilibria and periodic orbits are shown as dotted lines. The bifurcation values for  $a$  and the transitions are further discussed in the text. As before, the diagram was created using the MatContM software for discrete map iterations.

the right and to the left of the line  $\text{Re}(z) = -1$ , see Fig. 6a). On the other hand, when raising  $a$  in the positive range, the tail of the  $z_2$  Mandelbrot set shortens, so that past the high critical state  $a = 0.7$ , the point  $c = -1$  is left out, and the whole set is to the right of the line  $\text{Re}(z) = -1$  (see Fig. 6b). Along this interval, there are values of  $a$  for which the node  $z_2$  has a super-attracting orbit at  $c = -1$  (for example, the critical orbit is periodic at  $a = -2$ ,  $a = -1.6$ ,  $a = -1$ ,  $a = 0$ ,  $a = 1/5$ ,  $a = 0.3$ ). There are also values of  $a$  for which the  $z_2$  component of the critical orbit is pre-periodic at  $c = -1$  ( $a = -0.5$ ).

One can then further look at the third component of the critical orbit corresponding to the node  $z_3$ . For example, in the case when the critical orbit of  $z_2$  stabilizes asymptotically to an attracting period two oscillation, this oscillation is represented by a fixed point  $\xi_0$  for the function  $f(\xi) = (\xi^2 - 1 - a)^2 - 1$  above. In this case, in order to study the asymptotic behaviour in the third node  $z_3$  under the original quadratic function that applies to this node, one can instead study the behaviour of the orbit formed by every fourth iteration of  $z_3$ , by considering the function  $g(\xi) = (\xi_0 + b\xi)^2 - 1$ . For  $\xi_0$  in the intervals found above, one can study asymptotic dependence on  $b$  as before, by constructing a bifurcation diagram similar to that constructed in Fig. 5.

We can use these observations to further investigate whether there is a relationship between how the former centres of hyperbolic components are being affected by perturbations in the network structure (i.e., whether they still belong to the equi-M set) and the connectedness of the equi-M set as a whole. Below, we try to understand this comparison, using a more comprehensive illustration of asymptotic behaviour within the particular three-dimensional family of feed-forward networks considered above. In Fig. 7a, we show the connectivity parameter locus  $(a, b)$  (represented along the horizontal and respectively vertical coordinate axes) for which the complex parameter  $c = -1$  is in the equi-M set. In Fig. 7b, we show the result of a rough computation of the number of connected components in the equi-M set, for each parameter pair  $(a, b)$ . Due to difficulty in the reduced resolution (that was necessary for ensuring feasible computation time), we used a ‘blow-up’ algorithm that expanded each equi-M set by a small margin before assessing its connectedness. While this may be introducing some negative error in detecting

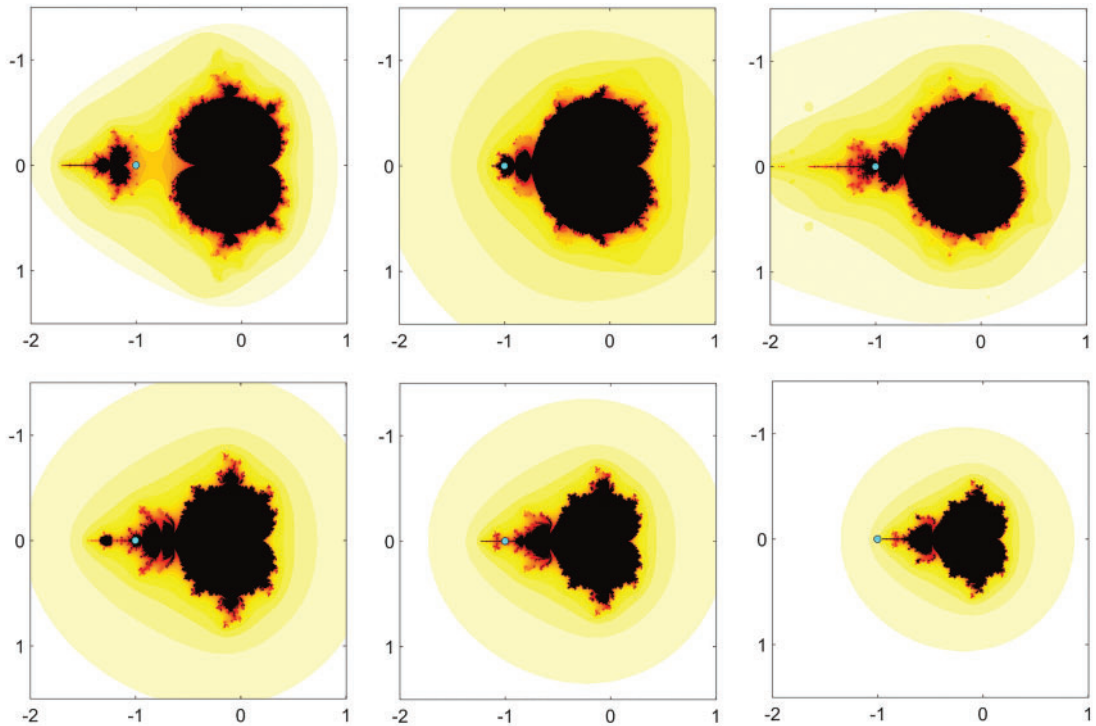


FIG. 6. Node-wise Mandelbrot sets for  $z_2$ , illustrated for different values of  $a$  along the bifurcation diagram in Fig. 4. In each equi-M set, the cyan dot represents the point  $c = -1$ . (Top) From left to right:  $a = -2.1$  (M-set is pinched at  $c = -1$  and  $z_2$  component of the critical point escapes);  $a = -1$  (super-attracting orbit of period two at  $c = -1$ );  $a = -0.5$  ( $z_2$  component of critical point is pre-periodic at  $c = -1$ ). (Bottom)  $a \sim 0.2$  (super-attracting orbit of period two at  $c = -1$ );  $a \sim 0.4$  (super-attracting orbit of period five at  $c = -1$ );  $a = 0.75$  (M-set falls short of  $c = -1$  and  $z_2$  component of the critical point escapes).

distinct connected components, we found that it substantially reduces positive detection error (due to the inability of the numerical code to identify filaments in the original equi-M sets represented in reduced resolution, as further explained in Appendix B).

It is interesting to reinterpret the bifurcation diagram in Fig. 4 in the broader context of Fig. 7a. The former represents the slice  $a = -1$  of the latter, so that one can observe the three black intervals for  $b$  along the vertical line  $a = -1$ , representing the three windows in the bifurcation diagram where the critical orbit is bounded for  $c = -1$ . It is also interesting, although less trivial, to compare the left and right panels of Fig. 7. Although the presence of  $c = -1$  in the equi-M set does not imply connectedness, it is clearly related to the connectedness locus, with a break in connectedness (around the yellow region representing the boundary between one and two connected components in Fig. 7a) seemingly related to the boundary of the inner white region in Fig. 7a, where  $c = -1$  is pinched out of the M-set).

#### 2.4 Fatou–Julia Theorem extended

In our previous work [20], we noticed that existence of uni-Julia sets with finitely many connected components breaks, in the case of networks, the connected/dust duality on which the Fatou–Julia Theorem is based in the traditional case of single iterated quadratic maps. We relied on a few numerical illustrations

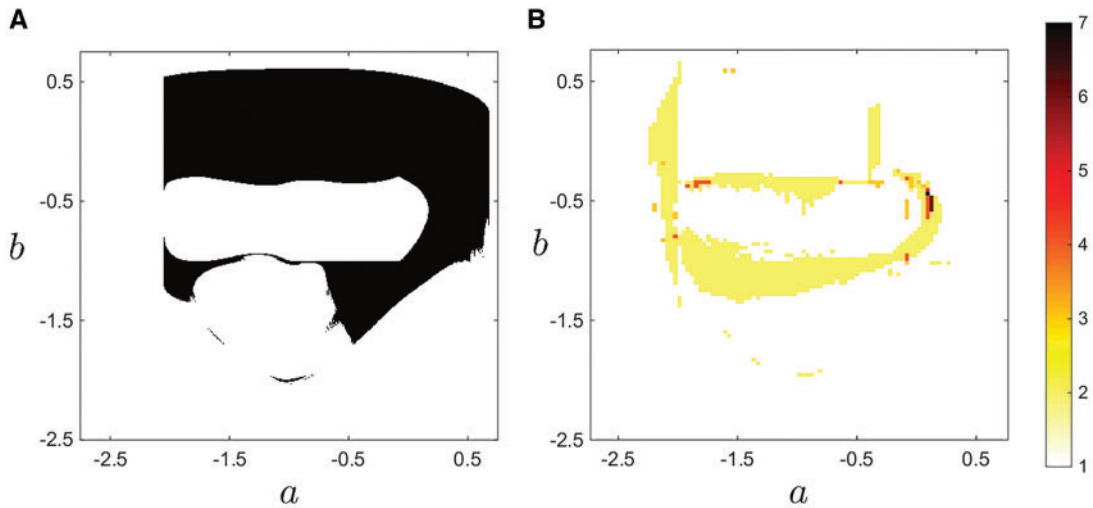


FIG. 7. Parameter loci in the  $(a, b)$  plane, for the network family given by:  $z_1 \rightarrow z_1^2 + c, z_2 \rightarrow (az_1 + z_2)^2 + c, z_3 \rightarrow (z_1 + z_2 + bz_3)^2 + c$ . (A) Locus (shown in black, computed within the rectangle  $[-2.75, 0.75] \times [-2.75, 0.75]$ ) of pairs  $(a, b)$  for which  $c = -1$  is in the equi-M-set. (B) Connectedness locus for the equi-M set, within the same rectangle  $[-2.75, 0.75] \times [-2.5, 0.75]$ , computed using the blowup algorithm before assessing connectivity of the sets. The colour corresponding to each  $c$  represents the estimated number of connected components of the equi-M set (as shown in the colour bar).

of uni-Julia sets for a variety of parameters  $c$ , chosen both inside and outside of the equi-M set for their respective network, to conjecture that the uni-J set is connected only if  $c$  is in the equi-M set of the network, and it is totally disconnected only if  $c$  is not in the equi-M set of the network.

Here, we illustrate this relationship in greater detail, while still using numerical approaches. In Fig. 8, we show the equi-M set for one of our self-drive example networks, together with a the uni-J sets corresponding to a collection of points  $c$  chosen close to the boundary of the equi-M set (so that some of them are inside the equi-M set, and some are outside). The illustration supports the idea that, although the connectivity of the uni-J sets (from one, to finitely many, to infinitely many components) degrades near the boundary of the M-set, there is no sudden break that happens precisely on the boundary, like in the case of single map iterations.

For a more systematic view, we computed and illustrated together, for a few example networks, the boundary of the equi-M set and the connectedness locus for the uni-J set. While the former was relatively easy to compute as the critically bounded locus for the network, the latter presented some difficulties in reconciling computational efficiency with obtaining uni-J sets in sufficiently good resolution to allow us to estimate their number of connected components. This was problematic in particular for the situations where the Julia set had short, thin filaments, likely to escape detection in low resolution, in which case we suspected the code to report ‘fake’ connected components, and thus over-count the number of components. To eliminate this positive error without increasing the  $z$ -plane resolution (which impacts computational time quadratically), we also used a common ‘blowup’ technique, adding a small border to each uni-J set to account for the possible connections due to filaments. This, of course, may introduce the opposite type of error (that of under-counting components). However, computations with and without blowup produced similar results qualitatively, in the sense of identifying the same loci of connectedness and total disconnectedness. In the transitional region, the connected component counts were higher with the first algorithm versus the second, as one would have expected (see Appendix B, Figs B1 and B2).

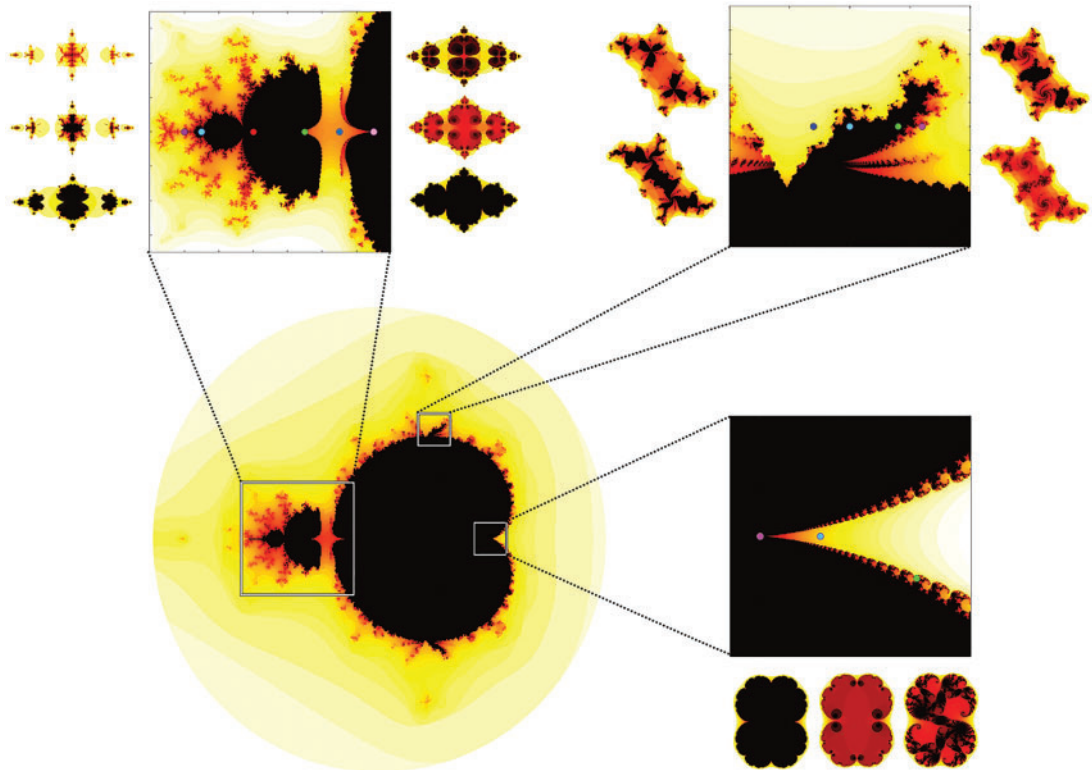


FIG. 8. Uni-Julia sets for a self-drive network with  $a = -1/3$  and  $b = -1/3$ , for different values of the equi-parameter  $c$ . We magnified three rectangular windows around the boundary of the network's equi-M set:  $[-0.2, 0.2] \times [0.245, 0.285]$  (around the cusp),  $[-0.2, 0] \times [0.58, 0.78]$  (top) and  $[-1.3, -0.6] \times [-0.3, 0.3]$  (around the tail). For each window, we show several uni-Julia sets corresponding to the  $c$  values marked in colours. For each magnification window, as the dots are listed from left to right, the corresponding uni-Julia sets are represented from left to right and then top to bottom.

In Fig. 9, we illustrate the implementation of the blow-up algorithm on the three self-drive networks shown in Fig. 2. We computed both the equi-M set in  $\mathbb{C}$  (in the sense defined in Section 1.3), as well as the connectedness locus (also in  $\mathbb{C}$ ) for the uni-J set of the network. While it does not come as a surprise that the two are no longer identical, we found that they are clearly related. Future work will focus on obtaining an analytic understanding of this relationship.

### 3. Network methods

#### 3.1 Spectral versus dynamic classes

For small or very simple networks, one can try to identify specifically the effect of different graph architectural properties on the ensemble asymptotic dynamics. As we have done in previous work for continuous time systems, we first investigate possible relationships between the network adjacency spectrum and the class of ensemble dynamics. For a network with discrete quadratic nodes, it seems natural to characterize the network by the properties of its asymptotic sets: the equi-M set and the uni-J set for a fixed equi-parameter  $c$ .

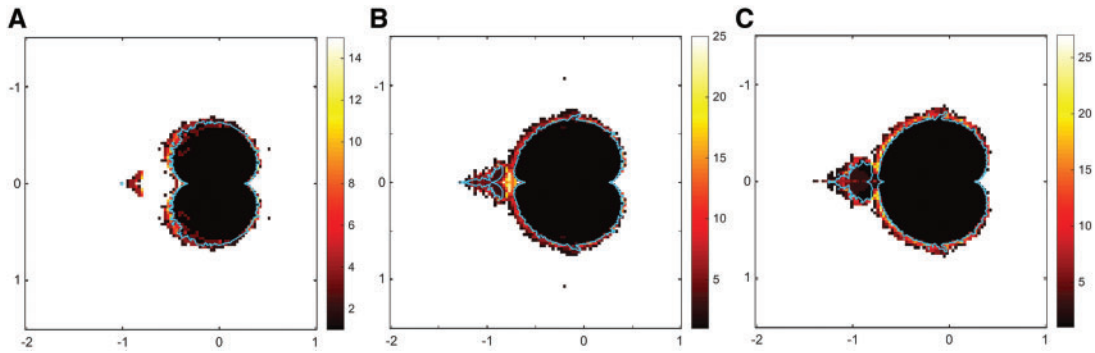


FIG. 9. Comparison between the equi-M set and the uni-J connectedness locus for the self-drive networks illustrated in Fig. 2. (A)  $a = -1$ ,  $b = -1$ ; (B)  $a = -1/3$ ,  $b = -1/3$ ; (C)  $a = -2/3$ ,  $b = -1/3$ . The panels represent the square  $[-2, 1] \times [-1.5, 1.5]$  in the equi-parameter plane. The cyan curve represents the boundary of the equi-M set, computed with 50 iterations. The colours correspond to the number of connected components for the respective uni-J set (computed approximately using the numerical algorithm discussed in Appendix B), with the colour scheme going from black (inside region, one connected component) through tones of red and yellow, as the number of connected components increases to 2, 3, etc. (see colour bar). White corresponds to the locus where the uni-J set was found to be dust (the numerical computations could not capture the totally disconnected points, so it returned the answer as ‘zero’ components, which we then scaled by hand to appear as white background).

**DEFINITION 3.1** We say that two networks  $\mathcal{N}_1$  and  $\mathcal{N}_2$  are in the same asymptotic class if, for any initial condition  $(z_0^1, z_0^2, \dots, z_0^N) \in \mathbb{C}^N$ , its multi-orbit under  $\mathcal{N}_1$  iterates out of the escape disc in the same number of iterations as when iterated under  $\mathcal{N}_2$ . We say that they are in the same uni-asymptotic class if the same applies for the multi-orbits of all initial conditions  $(z_0, z_0, \dots, z_0) \in \mathbb{C}^n$ .

**Remark.** Visually, this means that the corresponding prisoner sets (or uni-prisoner sets, respectively) are identical between two networks in the same uni-asymptotic class, and so are the escape sets, with identical ‘escape colours’ assigned to corresponding points.

**CONJECTURE 3.2** Within certain ranges of the equi-parameter  $c$ , network uni-asymptotic classes are invariant under changes in  $c$ .

The conjecture states a potentially very useful result: that two distinct configurations, which produce identical uni-asymptotic dynamics for one value of the parameter  $c$  will also do so for all any other value of  $c$  and two configurations, which produce different asymptotic structure under one value of  $c$  will still do so under any other value of  $c$ .

To investigate this hypothesis numerically, we focused on replicating the result in networks with two types of general restrictions: (1) networks with a fixed number of nodes  $N$  and a fixed number of edges  $j$ , with no additional conditions on the configuration; (2) bipartite networks with  $N$  nodes in each of the two interconnected cliques (previously used to represent interacting neural populations in our modelling work), and with specified number of edges  $i$  and  $j$  between the two cliques, respectively. In Appendix C, we illustrate one example from each category.

In Fig. C1, we considered all networks with  $N = 3$  nodes and  $j = 7$  edges, with all edge weights set as  $g = 1/N$ . The panels illustrate the uni-J sets for the equi-parameter values  $c = -1.15 + 0.26i$  and  $c = -0.13 + i$ . In Fig. C2, we considered all bipartite networks with  $N = 2$  nodes per clique,  $i = 1$  and  $j = 3$ , with positive weights  $g = 1/2$  for the edges connecting nodes within the cliques, and negative

weights  $g = -1/2$  for the edges between the cliques. The panels illustrate the uni-J and equi-M sets for the equi-parameter value  $c = -0.117 - 0.856i$ .

Spectral and asymptotic classes are not in a one-to-one correspondence, either way. Notice, in both tables, that two distinct matrices from the same spectral class may produce in some cases identical, in other cases different uni-asymptotic dynamics. Conversely, two matrices in different spectral classes may produce the same uni-asymptotic dynamics. However, even though not determined by the adjacency spectrum, uni-asymptotic classes remain consistent for all value of  $c$ .

### 3.2 Core asymptotic sets

In previous work, we have explored a statistical approach to relating graph structure to asymptotic dynamics in networks [7]. When interested in all network configurations with a specific property  $\mathcal{P}$  (e.g., density of oriented edges), one may consider, for each initial point (or alternately for each point in parameter space) the fraction of all configurations which produce a specific asymptotic behaviour. Then, a ‘probabilistic’ bifurcation can be defined in terms of the likelihood of a system to transition between two different behaviours when the edge configuration is slightly perturbed, given that the only knowledge we have on the network configuration is property  $\mathcal{P}$ .

For example, fix an equi-parameter  $c$ , and, for simplicity, set all edge weights in the network equal to  $1/N$ , where  $N$  is the size of the network. Consider the property  $\mathcal{P}$  to be fixing the number of edges to a positive integer  $k$ , with  $0 \leq k \leq N^2$ . For each  $z_0 \in \mathbb{C}$ , we count the fraction of configurations with  $\mathcal{P}$  for which the multi-orbit of  $(z_0, z_0, \dots, z_0)$  is bounded in  $\mathbb{C}^n$ .

**DEFINITION 3.3** We call the **core uni-prisoner set** the set of all points  $z_0 \in \mathbb{C}$ , for which the initial condition  $(z_0, \dots, z_0) \in \mathbb{C}^N$  produces a bounded multi-orbit when iterated under all network configurations with property  $\mathcal{P}$ . We call the **core uni-J set**<sup>1</sup> the boundary of this set in  $\mathbb{C}$ .

Instead of inspecting connectivity of each configuration-specific uni-J set at a time, one can instead study topological properties of the level sets of  $\mathcal{P}$  in the complex  $z$ -plane, in particular connectivity of the core uni-J set (which is the boundary of the 1-level set). One can track how the core uni-J set is affected when changing the edge weights  $g$ , the equi-parameter  $c$ , the network size  $N$  or, finally, even the network fixed property  $\mathcal{P}$ . Furthermore, one can distinguish between the parameter values for which the core uni-Julia set remains connected for all edge configurations with property  $\mathcal{P}$ , versus parameter values for which changes in edge density alter connectivity of the core uni-J set.

To fix our ideas, we discuss the concept of core uni-J set in the case of property  $\mathcal{P}$  being ‘fixed edge density  $\delta = k/N^2$ ’. Figures 10 and 11 illustrate core uni-J sets in networks of size  $N = 3$  and uniform edge weights  $g = 1/3$ , for different equi-parameters  $c$ , and different edge densities  $\delta$ . The colour associated to each point  $z_0 \in \mathbb{C}$  represents the likelihood (over all network configurations) for the initial condition  $(z_0, z_0, z_0)$  to remain bounded under iterations of a network with node-wise dynamics specified by  $c$  and edge density specified by  $\delta$ . In particular, the black central region represents the core uni-prisoner set. For example, Fig. 10a and b show the core Julia sets corresponding to the two classes of asymptotic dynamics described respectively in the left and right columns of Fig. C1 in Appendix C.

<sup>1</sup> This term was chosen in order to emphasize the analogy with a similar concept defined by Sumi in the case of random iterations of post-critically bounded polynomials [32, 33]

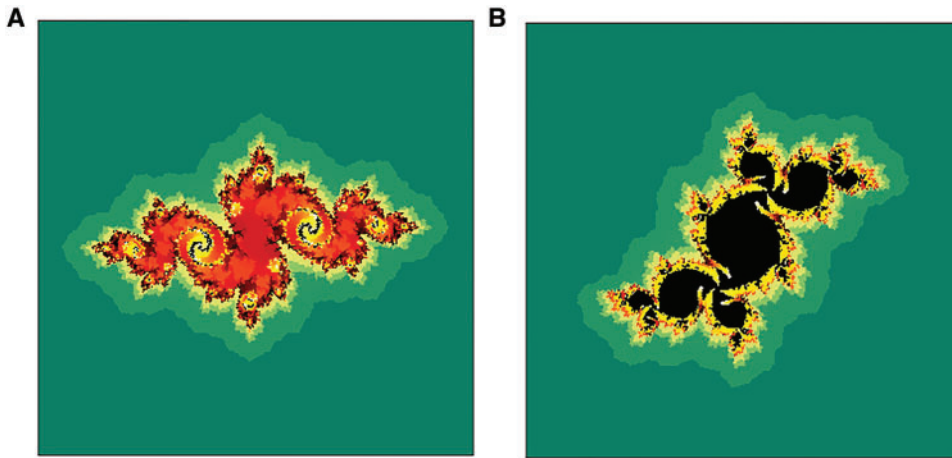


FIG. 10. Core uni-J sets over all network configurations with  $N = 3$  nodes, edge density  $\delta = 7/9$ , for fixed edge weights  $g = 1/3$ , and fixed equi-parameter  $c$ . (A)  $c = -1.15 + 0.26i$ ; (B)  $c = -0.13 + i$ . All panels were computed for 50 iterations, with spatial resolution  $200 \times 200$ , and escape radius  $R_e = 20$ . The colours code likelihood values from one (black) to zero (cyan), via intermediate values represented in red and yellow tones.

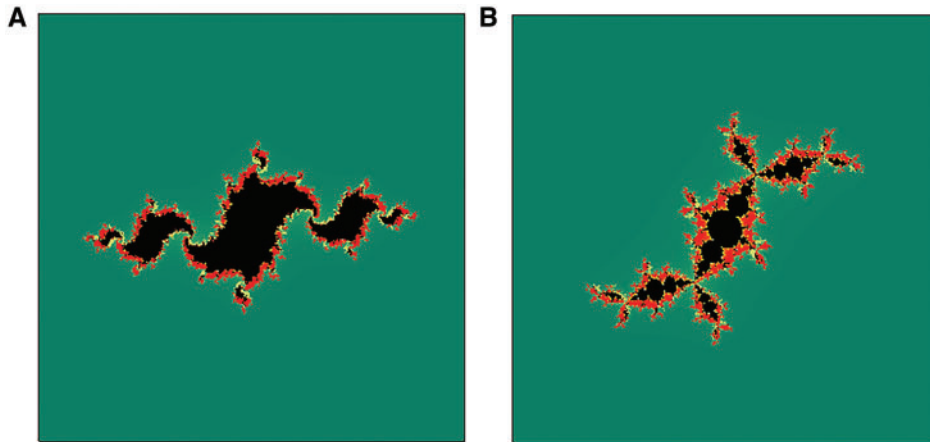


FIG. 11. Core uni-J sets over all network configurations with  $N = 3$  nodes, edge density  $\delta = 8/9$ , for fixed edge weights  $g = 1/3$ , and fixed equi-parameter  $c$ . (A)  $c = -1.15 + 0.26i$ ; (B)  $c = -0.13 + i$ . All panels were computed for 50 iterations, with spatial resolution  $200 \times 200$ , and escape radius  $R_e = 20$ . The colour coding is the same as in Fig. 10.

Intuitively speaking, as one would expect, the network dynamics becomes generally more rigid for higher edge densities  $\delta$ , and more fluid for lower densities, since more edges are expected to increase communication and ‘synchronization’ between nodes. This effect is clearly captured in the comparison between the lower density  $\delta = 7/9$  panels in Fig. 10, and the corresponding panels for the next higher density  $\delta = 8/9$  in Fig. 11. The level curves appear closer together in the case of higher density, so that small perturbations in the initial condition can more dramatically change the likelihood of a multi-orbit to escape. At a finer level, however, one can clearly notice that the effect of increasing the edge density  $\delta$  on the core uni-J set varies with the network. For example, depending on the equi-parameter  $c$ , the core uni-prisoner set may gain in area and connectedness with increasing edge density (as seen in left panels

of the two figures), or may shrink (as in the right panels). One can define and investigate the same concept similarly in equi-M sets:

**DEFINITION 3.4** We call the **core equi-M set** the set of all points  $c \in \mathbb{C}$  for which the critical multi-orbit is bounded in  $\mathbb{C}^n$ , when computed for all network configurations with property  $\mathcal{P}$ .

For small networks, the equi-M set is highly sensitive to small changes in the network architecture, as one can see for example in the Appendix C illustrations. By simply adding, deleting or moving one single edge, one can transition between asymptotic classes, thus altering substantially the geometry and properties of the equi-M set, and of the uni-J sets for all values of the parameter  $c$ . One is interested to ask the same type of questions in the context of higher-dimensional networks. Do small perturbations in the architecture affect the asymptotic behaviour to a similar extent, or do the rest of the edges stabilize the network? Does the presence of this ‘vulnerability’ depend on global properties such as overall edge density, or on local information, such as on the place where the addition/removal happened? These are important theoretical questions which relate to counterparts in modelling and the life sciences.

In Fig. 12, we show a core uni-J set and the core equi-M set for the collection of all networks of  $N = 10$  nodes, with  $\mathcal{P}$  being common edge density  $\delta = 80/100$ . The total number of configurations with property  $\mathcal{P}$  is extremely large (for the network size  $N = 10$ , which is still relatively small, one obtains  $\binom{100}{80}$ , which is of the order  $10^{20}$ ). Even considering the equivalence classes of asymptotic dynamics (assuming we have identified them and their size), averaging over all possibilities is extremely challenging computationally. In our previous work, we have shown that sample-based means are quite accurate, even for very small samples. In Fig. 12, we used samples of size  $\mathcal{S} = 20$  configurations out of the total of approximately  $5 \times 10^{20}$  to illustrate our core sets.

These types of illustrations offer concomitant (while sample-based) stochastic information on the asymptotic dynamics within a large collection of networks. They could be important in that they may

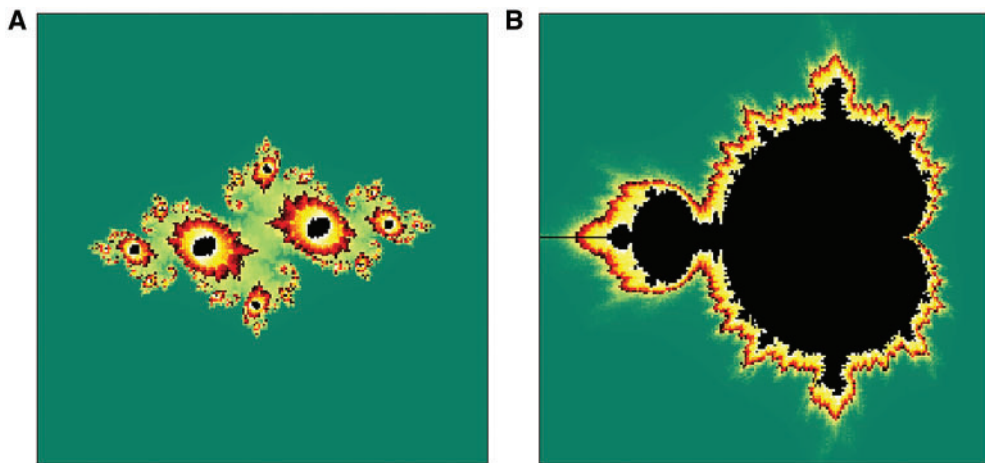


FIG. 12. Core sets for network configurations with  $N = 10$  nodes. (Left) Core uni-J set for fixed equi-parameter  $c = -1.15 + 0.26i$ , edge density  $\delta = 80/100$ , and fixed edge weights  $g = 1/N$ . (Right) Core equi-M set for edge density  $\delta = 60/100$  and edge weights  $g = 1/N$ . All panels were computed for  $k = 50$  iterations, with spatial resolution  $200 \times 200$ , and escape radius  $R_e = 20$ . The colour coding is the same as in Fig. 10.

help detect asymptotic properties which are robust to changes in architecture, and distinguish them from those which are sensitive to change. For example, one of the features which we had previously noticed consistently is the persistence of the cusp structure in all equi-M sets (with small variations in its position, depending on network architecture and node-wise dynamics). Figure 12b confirms this observation, showing minimal variability in the cusp area compared to regions of high sensitivity, such as the tail area, where even a small change in  $c$  may lead from certainty (black) to very small likelihood (yellow and red) of a bounded critical orbit.

## 4. Discussion

### 4.1 *Specific comments*

In this article, we reformulated some well-known questions from single map quadratic dynamics in the context of iterations of ensemble quadratic maps, coupled up in a network, according to an underlying adjacency graph structure. We investigated whether single map results regarding orbit convergence, escape radius and the topological structure of asymptotic sets change when studying a small network of  $n$  quadratic complex nodes. We focused in particular on one-dimensional complex slices of these sets in  $\mathbb{C}^n$ , which we called uni-J sets and equi-M sets.

We found that some of the structure of the traditional Mandelbrot set is conserved in network Mandelbrot slices, such as fractality on the boundary, or the presence of a cusp at its rightmost point along the real axis. It is interesting that the cusp seems persistent under changes in both network configuration, as shown in our previous article [20]) and set of weights, as shown in the current study (even though its position varies slightly with these parameters). In contrast, other features of the equi-M set are not as robust. We showed, for example, that the tail of the set is really fragile to perturbations in both configuration and weights. Equi-M sets no longer exhibit the traditional hyperbolic bulb structure and are not necessarily connected. Depending on the architecture of the network and the strength of the connections between nodes, the original centres of the hyperbolic components may no longer be within the equi-M set altogether. This affects in particular the tail of the set, where the former hyperbolic bulb with centre  $c = -1$  may pinch and break under slight perturbations of the weights in a certain range, as shown by our bifurcations diagrams.

Since one of our aims is to use the topological properties of the network equi-M set for classification purposes, it is important to understand where these properties are likely to change. To address this, we computed the equi-M set connectivity locus in a slice of the parameter space of weights. Since testing for connectivity is computationally more expensive and less reliable, we investigated the relationship between the connectivity of the equi-M set and the reshaping of the former hyperbolic bulbs. We observed in particular the deterioration of the bulb centred at  $c = -1$ , and related the parameter locus (in the space of weights) for which the network with nodes  $c = -1$  is post-critically bounded to the connectedness locus of the equi-M set. We found that the boundaries of these two parameter loci agree to some extent, but not enough to justify using the presence of  $c = -1$  in the equi-M set as an alternative test for connectedness of the equi-M set. Future work towards this goal may involve further study of the relationship between the integrity of the former hyperbolic components and connectedness of the equi-M set.

Another question we explored in this study is whether any relationship can be drawn (for fixed network configuration and weights) between the equi-M set and the Julia set connectedness locus. Their interplay is a lot more complicated in networks than the well known result for single map iterations. We investigated numerically a variant of this result. Since relating the network Julia and Mandelbrot sets as loci in  $\mathbb{C}^n$  is a more difficult computational problem, which may warrant a separate study, here we started by comparing the structure of the equi-M slices with the connectedness locus of the two-dimensional

uni-Julia sets (which are both sets in  $\mathbb{C}^2$ ). Our simulations, supporting previous work on this question, suggested that a gradual break in connectedness of the uni-J sets occurs near the boundary of the equi-M set. In other words, all  $c$  values which deliver connected uni-J sets lie in a region within the interior of the equi-M set, and all  $c$  values corresponding to totally disconnected uni-J sets are in a region contained in the complement of the equi-M set. The space between these two regions contains the boundary of the equi-M set, and is the locus of  $c$  values for which the uni-J set has a finite number of connected components. A more precise, qualitative description of this transitions requires an analytic approach that is the focus of our future work.

While, as illustrated by the examples considered in this article, analytic work is quite possible and seems promising in the case of small networks, it is likely that obtaining any useful results for higher-dimensional systems will require different, or additional techniques. We presented two possible approaches, one based on classification, and one based on statistics.

A few simulations found network structures which have identical asymptotic dynamics which continue to do so under changes of the quadratic parameter  $c$  within a certain range. This is interesting, since it suggests that, within a certain parameter locus, some information on the long-term outcome in a dynamic network is wired into the architecture, rather than in the node-wise dynamics. However, it is likely that this property is not general, but rather confined to a specific locus of  $c$  values, possibly related to the equi-M connectivity locus. Since this is a very important feature, which may help with the difficult problem of differentiating between the effects of configuration and those of node-wise dynamics, we will consider it more specifically in a separate project, as described in Section 4.2.

Our other proposed approach to large networks is to consider an ‘average’ view of asymptotic dynamics. This expands on previous work on continuous-time networks [7], where we defined a probabilistic version of bifurcation diagrams to simultaneously study the asymptotic behaviour of a large number of configurations. Similarly, in the case of discrete dynamics, one can consider a set of configurations characterized by a common property  $\mathcal{P}$  (e.g., edge density, or number of a certain motif) and count the fraction of those which produce a certain behaviour (e.g., post-critically bounded). One can construct in this fashion core uni-Julia and equi-Mandelbrot sets, and study how these vary when changing the property  $\mathcal{P}$  of the configuration.

#### 4.2 General comments and future work

We have chosen to study discrete networks of quadratic maps because they present well-posed, feasible mathematical problems. As we have mentioned in the Introduction, the same questions can easily become intractable when using more complicated node dynamics. This supports the strategy of using such simple models to begin understanding the behaviour of more complex systems, in which direct results are otherwise unreachable. When using a simple model of quadratic networks, one can put results in the perspective of the long-standing work with single-node iterations, and better understand the mechanisms of transition between a simple system with one operating unit and a complicated dynamic ensemble.

One natural course to follow from this point is to investigate which of the answers that we are obtaining in networks of quadratic nodes can be extended to other types of networks. We do not expect all our results to be universal, especially since some of our measures and techniques pertain specifically to complex maps. From the viewpoint of applications, we are primarily interested in further understanding the classification aspects, and then comparing them across networks with different types of node dynamics. A gradual, step by step investigation path may start by checking if the classification carries through for node-wise tent maps (as a canonical choice for a unimodal family), then for threshold linear maps (where we can compare with the results obtained by Curto *et al.* [9]), then for piecewise linear maps approximating

a sigmoidal function (in the manner of Caiola *et al.* [8]), then finally for standard Wilson-Cowan type nonlinear nodes (which triggered the original question and relates directly to many applications).

In this study, we suggested that a statistical outlook on classifying asymptotic dynamics may be efficient in describing networks with a prescribed architectural property. Another approach to resolving network complexity in a computationally practical way is to reduce the dimensionality of the graph while preserving the dynamics, by collapsing specific sets of nodes to single nodes. For example, as suggested in our prior research, in a graph with communities, rich clubs or strong components (within which the nodes are more tightly connected), it is possible that the dynamics is more robust to changes of structure *within* these modules, and more vulnerable to changes in the coupling *between* the modules. Then, we will investigate the possibility of classifying the ensemble dynamics based on simplified representations of the underlying graph, obtained by identifying the robust formations to simple nodes. This can reduce the classification problem to a working framework of much simpler graphs (e.g. trees, cycles), and would also offer a plausible explanation to the preference of natural systems for such hierarchic structures.

Another possible direction in our future work is aimed at investigating a somewhat different temporal coupling scheme for networks, built on principles of random iteration (reminiscent of Markov chains). From each node  $j$ , there is a probability  $p_{jk}$  for the information to travel along the outgoing edge  $E_{jk}$  to the adjacent node  $k$ , so that  $z_j$  will be iterated according to the map  $z_k(t) \rightarrow z_k(t+1)$  attached to that respective node. This defines a random  $n$ -dimensional iteration on  $(z_1, z_2, \dots, z_n)$ . The probabilities  $p_{jk}$  are nonzero only when there is an oriented edge connecting  $z_j$  and  $z_k$ . Additionally, the probabilities out of each node (including self cycles) have to add up to one:  $\sum_{k=1}^n p_{jk} = 1$ . Comerford [34] and Sumi [35] have made, for the past ten years, major contributions to the field of random iterations in the one-dimensional case, proving convergence of the Julia sets under random iterations of hyperbolic polynomial sequences, and describing a phenomenon of cooperation between generating maps as a factor decreasing the chaos in the overall system [36]. The extension of any of these concepts and results to dynamic networks would be not only mathematically significant, but also of potentially crucial interest to studying networks in the life sciences which may be governed precisely by these rules.

Finally, an extension with potentially high relevance to computational neuroscience would be introducing time and state-dependent edge weights. One of the most fundamental rules in neurobiology, quantifying the plasticity of brain connections that underlies processes like learning and memory formation, is Hebb's rule. In its most general form, the rule states that the system strengthens connections between neuron/nodes which have correlated (hence potentially causal) activity. One of the simplest historical implementations of Hebb's rule has been to adjust the weight of the each edge by a 'learning' term proportional to the product of the states of the adjacent nodes, at each iteration step. Then the dynamics of the system of network edge weights becomes as significant as the dynamics of the nodes themselves, with which they are coupled. The weights converge to an attracting state when the network has learned a certain configuration.

## Funding

This study was funded by the SUNY New Paltz Research, Scholarship and Creative Activities, by the SUNY New Paltz Research and Creative Project Awards, as well as by the New Paltz Foundation (Robert Kyncl '95 & Luz Avila Kyncl '96 STEM Exp Learning Fund).

## REFERENCES

1. BULLMORE, E. & SPORNS, O. (2009) Complex brain networks: graph theoretical analysis of structural and functional systems. *Nat. Rev. Neurosci.*, **10**, 186.
2. SPORNS, O. (2011) The non-random brain: efficiency, economy, and complex dynamics. *Front. Comput. Neurosci.*, **5**, 5.

3. SPORNS, O. (2003) Graph theory methods for the analysis of neural connectivity patterns. *Neuroscience Databases* (R. Kotter ed.). Boston, MA: Springer, pp. 171–185.
4. BRUNEL, N. (2000) Dynamics of sparsely connected networks of excitatory and inhibitory spiking neurons. *J. Comput. Neurosci.*, **8**, 183–208.
5. WILSON, H. R. & COWAN, J. D. (1972) Excitatory and inhibitory interactions in localized populations of model neurons. *Biophys. J.*, **12**, 1–24.
6. BORISYUK, G. N., BORISYUK, R. M., Khibnik, A. I. & ROOSE, D. (1995) Dynamics and bifurcations of two coupled neural oscillators with different connection types. *Bull. Math. Biol.*, **57**, 809–840.
7. RDULESCU, A. & VERDUZCO-FLORES, S. (2015) Nonlinear network dynamics under perturbations of the underlying graph. *Chaos*, **25**, 013116.
8. CAIOLA, M. & HOLMES, M. H. (2018) Model and analysis for the onset of parkinsonian firing patterns in a simplified basal ganglia. *Int. J. Neural Syst.*, pp. 1850021.
9. CURTO, C., GENESON, J. & MORRISON, K. (2018) Fixed points of competitive threshold-linear networks. Preprint arXiv:1804.00794.
10. ERMENTROUT, G. B. & KOPELL, N. (1986) Parabolic bursting in an excitable system coupled with a slow oscillation. *SIAM J. Appl. Math.*, **46**, 233–253.
11. BRUNEL, N. & LATHAM, P. E. (2003) Firing rate of the noisy quadratic integrate-and-fire neuron. *Neural Comput.*, **15**, 2281–2306.
12. HAUPTMANN, C., TOUCHETTE, H. & MACKEY, M. C. (2003) Information capacity and pattern formation in a tent map network featuring statistical periodicity. *Phys. Rev. E*, **67**, 026217.
13. JULIA, G. (1918) Memoire sur l'iteration des fonctions rationnelles. *J. Math. Pures Appl.*, **7**, 47–245.
14. FATOU, P. (1919) Sur les équations fonctionnelles. *Bull. Soc. Math. France*, **47** 1920.
15. MANDELBROT, B. B. (1980) Fractal aspects of the iteration of  $z \lambda z (1-z)$  for complex  $\lambda$  and  $z$ . *Ann. N. Y. Acad. Sci.*, **357**, 249–259.
16. BROOKS, R. & MATELSKI, J. P. (1981) The dynamics of 2-generator subgroups of  $psl(2, c)$ . *Riemann Surfaces and Related Topics: Proceedings of the 1978 Stony Brook Conference* (I. Kra & B. Maskit eds). Annals of Mathematics Studies, Princeton University Press, vol. 97. pp. 65–71.
17. BRANNER, B. & HUBBARD, J. H. (1992) The iteration of cubic polynomials part ii: patterns and parapatterns. *Acta Math.*, **169**, 229–325.
18. BONIFANT, A., KIWI, J. & MILNOR, J. (2010) Cubic polynomial maps with periodic critical orbit, part ii: escape regions. *Conform. Geom. Dynam.*, **14**, 68–112.
19. QIU, W. & YIN, Y. (2009) Proof of the branner-hubbard conjecture on cantor julia sets. *Sci. China Ser. A Math.*, **52**, 45–65.
20. RĂDULESCU, A. & PIGNATELLI, A. (2017) Real and complex behavior for networks of coupled logistic maps. *Nonlinear Dynam.*, **87**, 1295–1313.
21. BRANNER, B. (1989) The mandelbrot set. In *Chaos and fractals: the mathematics behind the computer graphics* (R. Devaney & L. Keen eds). *Proc. symp. appl. math.*, vol. 39. Providence, RI: American Mathematical Society, pp. 75–105.
22. JONSSON, M. (1999) Dynamics of polynomial skew products on  $\mathbb{C}^2$ . *Math. Ann.*, **314**, 403–447.
23. HEINEMANN, S.-M. (1998) Julia sets of skew products in  $\mathbb{C}^2$ . *Kyushu J. Math.*, **52**, 299–329.
24. PETERS, H. & MARJAN SMIT, I. (2017) Fatou components of attracting skew-products. *J. Geomet. Anal.*, **28**, pp. 84–110.
25. ROEDER, R. (2011) A dichotomy for Fatou components of polynomial skew products. *Conform. Geom. Dynam.*, **15**, 7–19.
26. MANÉ, R., SAD, P. & SULLIVAN, D. (1983) On the dynamics of rational maps. *Annales Scientifiques de l'École Normale Supérieure*, vol. 16. Gauthier-Villars (Editions Scientifiques et Medicales Elsevier), pp. 193–217.
27. LYUBICH, M. (1997) Dynamics of quadratic polynomials, i–ii. *Acta Math.*, **178**, 185–297.
28. GRACZYK, J. & SWIATEK, G. (1997) Generic hyperbolicity in the logistic family. *Ann. Math.*, **146**, 1–52.
29. DOUADY, A. & HUBBARD, J. H. (1984) Etude dynamique des polynomes complexes (Premiere partie). *Publications Mathematiques D'Orsay*. France: Université de Paris Sud. Orsay.
30. HUBBARD, J. (1992) *Local Connectivity of Julia Sets and Bifurcation Loci: Three Theorems of J.-C. Yoccoz*. Topological Methods in Modern Mathematics, Bures-sur-Yvette, France: Institut des Hautes Etudes Scientifique.

31. GOVAERTS, W., KUZNETSOV, Y. A., KHOSHSIAR GHAZIANI, R. & MEIJER, H. G. E. (2008) *Ci matcontm: A Toolbox for Continuation and Bifurcation of Cycles of Maps*. The Netherlands: Universiteit Gent, Belgium, and Utrecht University.
32. SUMI, H. (2006) Semi-hyperbolic fibered rational maps and rational semigroups. *Ergod. Theor. Dyn. Syst.*, **26**, 893–922.
33. SUMI, H. (2015) Random complex dynamics and devil’s coliseums. *Nonlinearity*, **28**, 1135.
34. COMERFORD, M. (2006) Hyperbolic non-autonomous julia sets. *Ergod. Theor. Dyn. Syst.*, **26**, 353–377.
35. SUMI, H. (2001) Dynamics of sub-hyperbolic and semi-hyperbolic rational semigroups and skew products. *Ergod. Theor. Dyn. Syst.*, **21**, 563–603.
36. SUMI, H. Random complex dynamics and semigroups of holomorphic maps. *Proc. Lond. Math. Soc.*, **102**, 50–112.

## Appendix A

LEMMA .1 The point  $c = -3/4$  is not in the equi-M set for the network given by:  $z_1 \rightarrow z_1^2 + c$ ,  $z_2 \rightarrow (az_1 + z_2)^2 + c$ ,  $z_3 \rightarrow (z_1 + z_2 + bz_3)^2 + c$ , with connectivity weights  $a = -1$ ,  $b = -1$ .

*Proof.* It is easy to see that the interval  $[-3/4, 0]$  is invariant under the iteration of the function  $z_1 \rightarrow z_1^2 - 3/4$  (since the minimum value of the function  $f(z) = z^2 - 3/4$  for  $z \in [-3/4, 0]$  is  $f(0) = -3/4$ , and the maximum value is  $f(-3/4) = -3/16 < 0$ ). Since  $z_1(0) = 0 \in [-3/4, 0]$ , it follows by induction that  $z_1 \in [-3/4, 0]$  for all iterates, hence the first node is bounded.

We will show, using induction, that  $-3/4 \leq z_2 \leq 0$  also for all iterates. This is satisfied for  $z_2(0) = 0$ . Suppose that  $z_2(t) \in [-3/4, 0]$  for some  $t \geq 0$ ; we will show that  $z_2(t+1)$  is also within this interval. We know that  $-3/4 \leq z_1(t) \leq 0$ , and  $-3/4 \leq z_2(t) \leq 0$ , hence  $-3/4 \leq -z_1(t) + z_2(t) \leq 3/4$ , and  $0 \leq (-z_1(t) + z_2(t))^2 \leq 9/16$ . Then  $z_2(t+1) \in [-3/4, -3/16] \subset [-3/4, 0]$ , which concludes the induction and shows that the critical point  $z_2$  is bounded. Moreover, since  $z_1, z_2 \in [-3/4, 0]$ , it follows that  $-1 \leq z_1 + z_2 + 1/2 \leq 1/2$ , hence  $|z_1 + z_2 + 1/2| \leq 1$ , which we will use below.

It is easy to calculate that the orbit of  $z_3$  grows relatively fast for the first portion of the iteration, so that  $z_3(8) > 5$ . We will use this to show that, in fact, the orbit of the third node escapes to infinity. First notice that, for all iterates (in particular for  $t \geq 8$ ), we have:

$$|z_3(t+1)| = |(z_1 + z_2 - z_3)^2 - 3/4| \geq |(z_1 + z_2 - z_3)|^2 - 3/4$$

For simplicity, we left out the index for the current iterate (e.g.,  $z_1$  above represents  $z_1(t)$ ). This further implies that:

$$\sqrt{|z_3(t+1)| + 3/4} \geq |(z_1 + z_2 + 1/2) + (-z_3 - 1/2)| \geq |-z_3 - 1/2| - |z_1 + z_2 + 1/2|$$

Since  $|z_1 + z_2 + 1/2| \leq 1$ , we further have that

$$\sqrt{|z_3(t+1)| + 3/4} \geq |z_3| - 1/2 - 1 \geq |z_3| - 3/2$$

Since  $z_3 > 5$ , we can square both sides:

$$|z_3(t+1)| \geq (|z_3| - 3/2)^2 - 3/4$$

We want to show that  $(|z_3| - 3/2)^2 - 3/4 \geq 2|z_3|$ . Consider the quadratic function

$$f(\xi) = (\xi - 3/2)^2 - 3/4 - 2\xi = \xi^2 - 5\xi + 3/2,$$

with roots  $0 < \xi_1 < \xi_2 < 5$ . Since  $|z_3| > 5$ , it follows that  $f(|z_3|) > 0$ , hence

$$(|z_3| - 3/2)^2 - 3/4 - 2|z_3| > 0$$

It follows that, as needed

$$|z_3(t+1)| \geq 2|z_3(t)| \text{ for } t \geq 8$$

In conclusion, the node-wise orbit  $z_3$  escapes to infinity.  $\square$

## Appendix B

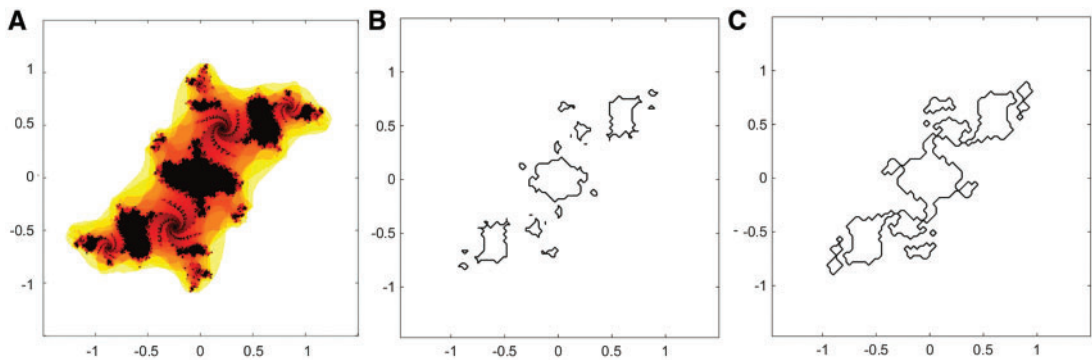


FIG. B1. Comparison between detection of connected components of uni-J sets, using the standard algorithm from the Matlab image processing toolbox versus an improved version including an initial blowup of the Julia set by a one pixel margin. (A) High resolution ( $400 \times 400$  pixels) Uni-J set for the self-drive network  $a = -2/3$ ,  $b = -1/3$ , corresponding to  $c = -0.06 - 0.68i$ ; (B) Count of connected components in low resolution ( $100 \times 100$  pixels) using the standard algorithm found 29 components; (C) Count of connected components in low resolution ( $100 \times 100$  pixels) using the improved algorithm found three components.

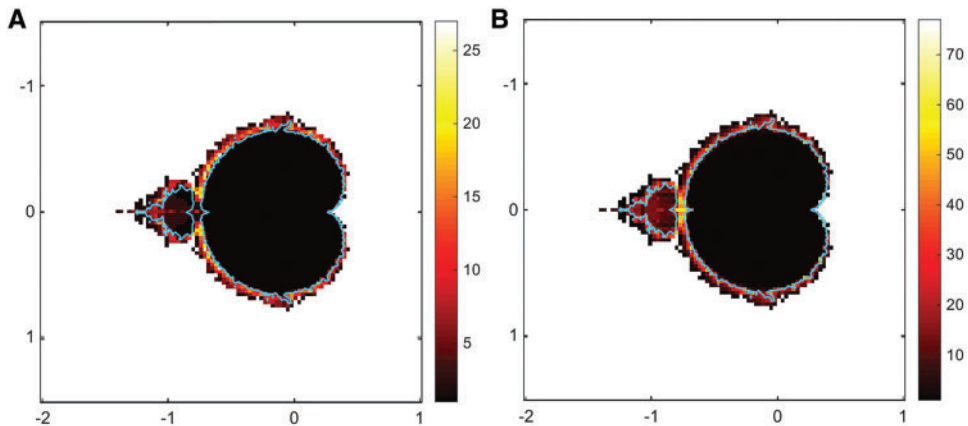


FIG. B2. Comparison between the uni-J set connectedness locus computed using a direct estimate of the number of connected components versus using the blowup technique. Both panels represent the square  $[-2, 1] \times [-1.5, 1.5]$  in the equi-parameter plane. The cyan curve represents the boundary of the equi-M set, computed with 50 iterations. The colours correspond to the number of connected components for the respective uni-J set, computed directly (left) versus using a blowup of 1.5 pixels for the Julia set (right). The panels are almost identical in the black (connected) and white (totally disconnected) regions, while the scale/ number of connected components are very different in the transitional coloured region (as shown by the ranges on the colour bars).

## Appendix C

$\begin{bmatrix} 1 & 1 & 1 \\ 1 & 1 & 0 \\ 1 & 1 & 0 \end{bmatrix}$ ( $\mathcal{A}_i$ )	$\begin{bmatrix} 1 & 1 & 0 \\ 1 & 1 & 1 \\ 1 & 1 & 0 \end{bmatrix}$ ( $\mathcal{A}_i$ )	$\begin{bmatrix} 1 & 1 & 0 \\ 1 & 1 & 0 \\ 1 & 1 & 1 \end{bmatrix}$ ( $\mathcal{B}_{iv}$ )
$\begin{bmatrix} 1 & 1 & 1 \\ 1 & 1 & 1 \\ 1 & 0 & 0 \end{bmatrix}$ ( $\mathcal{A}_{ii}$ )	$\begin{bmatrix} 1 & 1 & 1 \\ 1 & 1 & 0 \\ 1 & 0 & 1 \end{bmatrix}$ ( $\mathcal{C}_i$ )	$\begin{bmatrix} 1 & 1 & 0 \\ 1 & 1 & 1 \\ 1 & 0 & 1 \end{bmatrix}$ ( $\mathcal{D}_v$ )
$\begin{bmatrix} 1 & 1 & 1 \\ 1 & 0 & 1 \\ 1 & 1 & 0 \end{bmatrix}$ ( $\mathcal{E}_i$ )	$\begin{bmatrix} 1 & 1 & 1 \\ 1 & 0 & 0 \\ 1 & 1 & 1 \end{bmatrix}$ ( $\mathcal{A}_{ii}$ )	$\begin{bmatrix} 1 & 1 & 0 \\ 1 & 0 & 1 \\ 1 & 1 & 1 \end{bmatrix}$ ( $\mathcal{F}_{iii}$ )
$\begin{bmatrix} 1 & 1 & 1 \\ 1 & 0 & 1 \\ 1 & 0 & 1 \end{bmatrix}$ ( $\mathcal{A}_i$ )	$\begin{bmatrix} 1 & 0 & 1 \\ 1 & 1 & 1 \\ 1 & 1 & 0 \end{bmatrix}$ ( $\mathcal{F}_{iii}$ )	$\begin{bmatrix} 1 & 0 & 1 \\ 1 & 1 & 0 \\ 1 & 1 & 1 \end{bmatrix}$ ( $\mathcal{D}_v$ )
$\begin{bmatrix} 1 & 0 & 0 \\ 1 & 1 & 1 \\ 1 & 1 & 1 \end{bmatrix}$ ( $\mathcal{B}_{vi}$ )	$\begin{bmatrix} 1 & 0 & 1 \\ 1 & 1 & 1 \\ 1 & 0 & 1 \end{bmatrix}$ ( $\mathcal{B}_{iv}$ )	$\begin{bmatrix} 1 & 0 & 1 \\ 1 & 0 & 1 \\ 1 & 1 & 1 \end{bmatrix}$ ( $\mathcal{A}_i$ )
$\begin{bmatrix} 1 & 1 & 1 \\ 1 & 1 & 1 \\ 0 & 1 & 0 \end{bmatrix}$ ( $\mathcal{A}_{ii}$ )	$\begin{bmatrix} 1 & 1 & 1 \\ 1 & 1 & 0 \\ 0 & 1 & 1 \end{bmatrix}$ ( $\mathcal{D}_v$ )	$\begin{bmatrix} 1 & 1 & 0 \\ 1 & 1 & 1 \\ 0 & 1 & 1 \end{bmatrix}$ ( $\mathcal{C}_i$ )
$\begin{bmatrix} 1 & 1 & 1 \\ 1 & 1 & 1 \\ 0 & 0 & 1 \end{bmatrix}$ ( $\mathcal{B}_{vi}$ )	$\begin{bmatrix} 1 & 1 & 1 \\ 1 & 0 & 1 \\ 0 & 1 & 1 \end{bmatrix}$ ( $\mathcal{F}_{iii}$ )	$\begin{bmatrix} 1 & 0 & 1 \\ 1 & 1 & 1 \\ 0 & 1 & 1 \end{bmatrix}$ ( $\mathcal{D}_v$ )
$\begin{bmatrix} 1 & 1 & 1 \\ 0 & 1 & 1 \\ 1 & 1 & 0 \end{bmatrix}$ ( $\mathcal{F}_{iii}$ )	$\begin{bmatrix} 1 & 1 & 1 \\ 0 & 1 & 0 \\ 1 & 1 & 1 \end{bmatrix}$ ( $\mathcal{B}_{vi}$ )	$\begin{bmatrix} 1 & 1 & 0 \\ 0 & 1 & 1 \\ 1 & 1 & 1 \end{bmatrix}$ ( $\mathcal{D}_v$ )
$\begin{bmatrix} 1 & 1 & 1 \\ 0 & 1 & 1 \\ 1 & 0 & 1 \end{bmatrix}$ ( $\mathcal{D}_v$ )	$\begin{bmatrix} 1 & 1 & 1 \\ 0 & 0 & 1 \\ 1 & 1 & 1 \end{bmatrix}$ ( $\mathcal{A}_{ii}$ )	$\begin{bmatrix} 1 & 0 & 1 \\ 0 & 1 & 1 \\ 1 & 1 & 1 \end{bmatrix}$ ( $\mathcal{C}_i$ )
$\begin{bmatrix} 1 & 1 & 1 \\ 0 & 1 & 1 \\ 0 & 1 & 1 \end{bmatrix}$ ( $\mathcal{B}_{iv}$ )	$\begin{bmatrix} 0 & 1 & 1 \\ 1 & 1 & 1 \\ 1 & 1 & 0 \end{bmatrix}$ ( $\mathcal{E}_i$ )	$\begin{bmatrix} 0 & 1 & 1 \\ 1 & 1 & 0 \\ 1 & 1 & 1 \end{bmatrix}$ ( $\mathcal{F}_{iii}$ )
$\begin{bmatrix} 0 & 1 & 0 \\ 1 & 1 & 1 \\ 1 & 1 & 1 \end{bmatrix}$ ( $\mathcal{A}_{ii}$ )	$\begin{bmatrix} 0 & 1 & 1 \\ 1 & 1 & 1 \\ 1 & 0 & 1 \end{bmatrix}$ ( $\mathcal{F}_{iii}$ )	$\begin{bmatrix} 0 & 1 & 1 \\ 1 & 0 & 1 \\ 1 & 1 & 1 \end{bmatrix}$ ( $\mathcal{A}_i$ )
$\begin{bmatrix} 0 & 0 & 1 \\ 1 & 1 & 1 \\ 1 & 1 & 1 \end{bmatrix}$ ( $\mathcal{A}_{ii}$ )	$\begin{bmatrix} 0 & 1 & 1 \\ 1 & 1 & 1 \\ 0 & 1 & 1 \end{bmatrix}$ ( $\mathcal{A}_i$ )	$\begin{bmatrix} 0 & 1 & 1 \\ 0 & 1 & 1 \\ 1 & 1 & 1 \end{bmatrix}$ ( $\mathcal{A}_i$ )

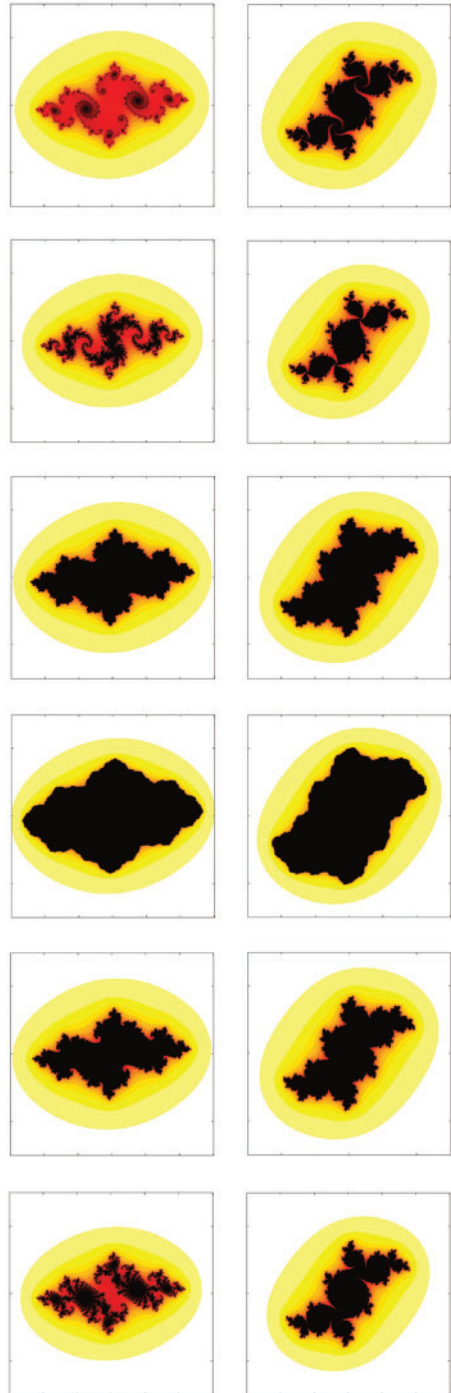


FIG. C1. Spectral classes versus asymptotic classes for all networks with  $N = 3$  nodes and  $j = 7$  edges. Spectral classes are designated by letters  $\mathcal{A} - \mathcal{F}$  for all adjacency matrices on the left; the asymptotic classes, designate by indices  $i-vi$ , are illustrated on the right for two distinct values of the equi-parameter:  $c = -1.15 + 0.26i$  (left column) and  $c = -0.13 + i$  (right column). The edge weights were fixed to  $g = 1/3$ . The figure panels show, top to bottom, all asymptotic classes  $i-vi$  and were created based on 100 iterations, in  $400 \times 400$  resolution.

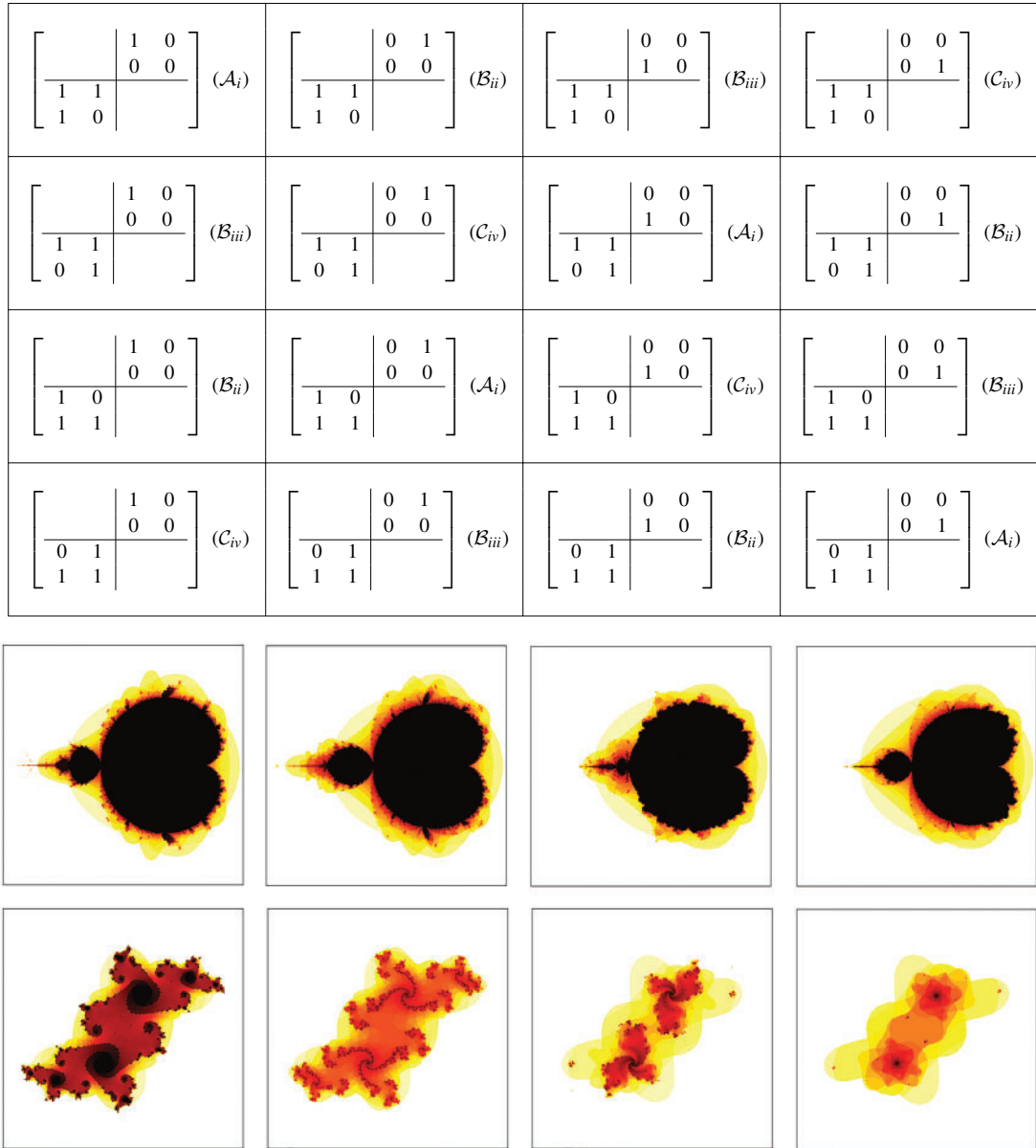


FIG. C2. Adjacency and dynamics classes for  $N=2$ , density type  $(M_{xy}, M_{yx})=(1,3)$  and  $g_{xx} = g_{yy} = 0.5, g_{xy} = g_{yx} = -0.5$ . Adjacency matrices are represented as block binary matrices, with the empty corners representing all 1 blocks. Spectral adjacency classes are designated by letters  $(\mathcal{A} - \mathcal{C})$  and asymptotic classes denoted by the subscript  $(i - iv)$ . The top figure panels represent the equi-M sets for all asymptotic classes  $i-iv$ . The bottom figure panels show the  $i-iv$  uni-planes for the equi-parameter ( $c = -0.117 - 0.856i$ ), with prisoners plotted in black and escapes plotted in colours according to the escape rate. Notice that in this case one can achieve all dynamics classes by changing either one of the diagonal block matrices, while keeping the other fixed.